Mühendislik Bilimleri ve Tasarım Dergisi
9(1), 27 – 51, 2021
e-ISSN: 1308-6693

Journal of Engineering Sciences and Design
DOI: 10.21923/jesd.861520

Araştırma Makalesi Research Article

THE STRUCTURAL COUPLING TO RUPTURE COMPLEXITY OF THE AFTERSHOCK SEQUENCE OF THE 2011 EARTHQUAKES IN LAKE VAN AREA (EASTERN ANATOLIA, TURKEY)

Mustafa TOKER*

Van Yuzuncu Yıl University, Faculty of Engineering, Department of Geophysical Engineering, Van,Turkey

Keywords

Lake Van, Van Earthquake, Aftershock Sequence, Microseismicity, Clusters.

Abstract

This study presents an analysis of the structural coupling to the two large destructive earthquakes that occurred in Lake Van area on October 23 (Mw 7.1), and November 9 (Mw 5.6), 2011, together with the azimuth-dependent distribution of the seismic activity and microseismicity clusters after the mainshocks, associated with the complex rupture processes of the aftershock sequence. The aftershock sequences after the two mainshocks were linked to the local crustal faults beneath Lake Van area, followed successively and produced unusually intense activity and significant damage in the area. The main purposes of this study are to document the spatial and temporal distribution and evolution of the October 23, 2011 aftershock hypocenters and the azimuth-dependent distribution of seismic activity, and to understand the structural character of the aftershock sequence using the distributional and evolutional patterns of the aftershock hypocenters. A total of 10,000 aftershocks were obtained from seismic data with a high signal-to-noise ratio collected over three years from October 23, 2011 to March 17, 2014. These aftershocks were relocated for the time periods from November 2011 through March 2012 to March 2014 and ≈ 5000 aftershocks were retained in the depth versus distance cross-sections to detect the clusters in the first step of study (November 2011-March 2012). The focal depth distribution of the aftershock clusters, the migration of hypocenter activity and microseismicity clusters were analyzed and the distributional patterns of the detected clusters were assessed using the geometric distribution of the aftershock hypocenters. The spatial and temporal distribution of aftershocks reveals interesting key features of the deep rupture complexity of the Van earthquake. This study presents the results of the first detailed hypocentral observations and this is important data for future seismic hazard analyses in the study area.

VAN GÖLÜ BÖLGESİNDE 2011 YILI DEPREMLERİNİN ARTÇI ŞOK SERİSİ KIRILMA KARMAŞIĞINA YAPISAL BAĞLANTI (DOĞU ANADOLU, TÜRKİYE)

Anahtar Kelimeler

Van Gölü, Van Depremi, Artçışok Sekansı, Mikrosismisite, Kümeler.

Öz

Bu çalışma, Van Gölü alanında gerçekleşen, 23 Ekim Van (Mw 7.1) ve 9 Kasım Edremit (Mw 5.6) 2011 yılı depremleriyle, artçışok kırılma karmaşığına bağlı olarak, anaşok sonrası oluşan küçük deprem kümelerinin ve genel sismik hareketliliğin, azimuta bağlı değişimini dikkate alarak kurulan yapısal ilişkinin bir analizini sunmaktadır. Her iki anaşoktan sonra oluşan artçışok serileri, Van Gölünün altında bulunan kabuk kökenli faylarla ilişkilendirilmiş ve ardarda olmak üzere, sıradışı yıkıcı bir etki oluşturarak, bölgede çok önemli bir zarara neden olmuşlardır. Bu nedenle, çalışmamızın temel amacı, 23 Ekim 2011 artçışok odak derinliklerinin zamana, mekana ve azimuta bağlı olarak dağılımını ve dağılım sürecini göstermek ve aynı zamanda, artçışok odak derinliklerini kullanarak, artçışok serilerinin yapısal karakterini anlamaktır. Bu çalışmada, yaklaşık 10.000 artçışok verisi, 23 Ekim 2011 ve 17 Mart 2014 tarihleri arasında 3 yıl süreyle kaydedilen, sinyal gürültü oranı yüksek deprem katalogundan elde edilmiştir. Bu artçışok veri seti, 2011 Kasım ve 2014 Mart tarihleri arasında yeniden yersel olarak konumlandırılmış ve bu çalışmanın ilk aşamasını teşkil eden, yaklaşık 5000 adet artçışok verisi, derinlik-uzaklık profil kesitlerinde, deprem kümelenmelerini tespit edebilmek için

* İlgili yazar / Corresponding author: tokermu@gmail.com, +90-432-444-5065

kullanılmıştır (Kasım 2011-Mart 2012). Böylece, artçışok kümelenmelerinin derinlik dağılımı, deprem odak derinliklerin hareketi ve küçük deprem kümelenmelerinin analizi gerçekleştirilmiştir ve ayrıca, artçışok odak derinliklerinin geometrik dağılımı kullanılarak, tespit edilmiş deprem kümelenmelerinin dağılım geometrilerinin analizi yapılmıştır. Artçışokların zamanda ve mekandaki dağılımları, Van depremini oluşturan fayın derinlerdeki kırılma karmaşasına dair, çok ilginç temel özelliklerini açıkça göstermiştir. Bu çalışma, ilk kez, deprem odağı analizi detaylı gözlem sonuçlarını vermektedir ve bu veri sonuçları, çalışma alanında, gelecekteki olması muhtemel deprem hasar analizleri için çok önem arz etmektedir.

Alıntı / Cite

Toker, M., (2021). The Structural Coupling to Rupture Complexity of the Aftershock Sequence of the 2011 Earthquakes in Lake Van Area (Eastern Anatolia, Turkey), Journal of Engineering Sciences and Design, 9 (1), 27-51.

Yazar Kimliği / Author ID (ORCID Number)	Makale Süreci / Article Process	
M. Toker, 0000-0001-9981-6605	**Başvuru Tarihi / Submission Date**	14.01.2021
	Revizyon Tarihi / Revision Date	13.02.2021
	Kabul Tarihi / Accepted Date	01.03.2021
	Yayım Tarihi / Published Date	30.03.2021

1. Introduction

During the last ten years, seismological observations of aftershock seismicity from the interplate and intraplate seismotectonic settings and magnitudes have indicated that variations in stress state less than 1 bar are able to induce the reactivation of nearby faults that are close to failure, either as long-term post-seismic deformation (e.g., spatial and temporal occurrence of aftershock activity) or as secondary larger earthquakes (e.g., compound seismicity). This phenomenon has been described as a triggering process (King et al. 1994; Harris et al. 1995; Benito et al. 2004). The triggering process may involve the anomalous generation of aftershocks or secondary mainshocks with different focal mechanisms, with prominent changes in the spatial and temporal character of the mainshock aftershock sequence in a given focal area which increases or decreases for several months or years after a mainshock (Stein and Lisowski 1983; Reasenberg and Simpson 1992; Stein 1999; Benito et al. 2004).

Lake Van located in the province of Van in eastern Anatolia is characterized by intraplate seismicity and highly active compressional shear strains (Kutoğlu et al. 2016) with long-term aftershocks of magnitudes more than 3.5-4.0 occurring repeatedly (Toker 2013; 2014) (Figure 1). Toker (2014; 2015) has shown that these aftershock events in the temporal form of multi-clusteral patterns are repeating ruptures of asperities comprising areas of large coseismic slip, which are locked during interseismic period. On October 23, 2011, a great thrust earthquake of magnitude Mw 7.1 occurred in the Lake Van area (Irmak et al. 2012; Bayrak et al. 2013; Elliott et al. 2013; Acarel et al., 2014; Gori et al., 2014; Moro et al. 2014; Toker 2015; Mackenzie et al., 2016) (Figure 1). The earthquake and its strong aftershocks activated the ~27-km-long Blind Thrust fault system that marks the accretionary wedge complex and the transition between the basins of Lake Van and Lake Erçek (Doğan and Karakaş 2013; Elliott et al. 2013; Karakaş et al. 2013; Doğan et al. 2014). The multi-crustal occurrence and distribution of long-period aftershocks and focal mechanism of this larger event show a northeast–southwest striking rupture plane dipping towards the northwest (Irmak et al. 2012; Toker 2013; Bayrak et al. 2013; Fielding et al. 2013; Utkucu et al. 2013; Gori et al., 2014; Mackenzie et al., 2016). The rupture gradually expanded near the hypocenter and was shaped in a sigmoidal-like propagation (Figure 1). It is thought that the earthquake occurred as a result of a long-term high plateau uplift (Görür et al. 2015) and an eastward oblique tectonic extrusion of the Lake Van basin (Toker and Şengör 2011; Toker and Ecevitoğlu 2012a, b; Toker, 2017; Toker et al., 2017).

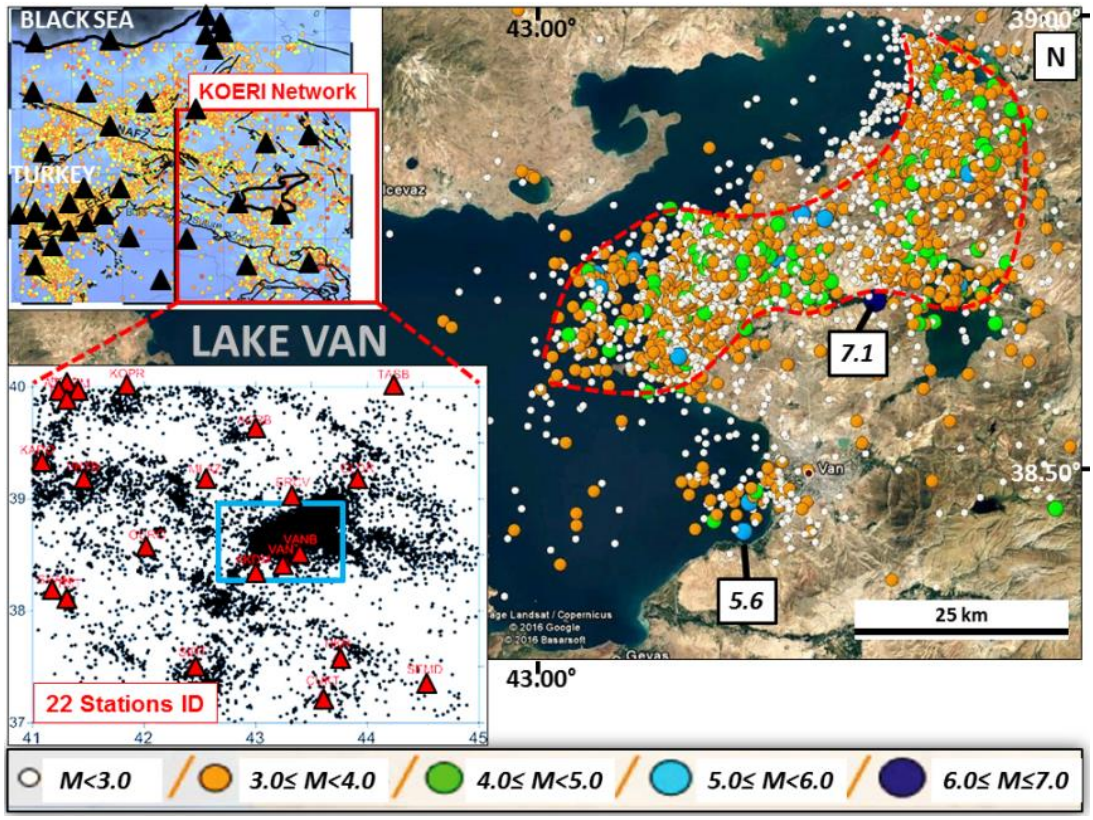

Figure 1. The catalogue seismicity of the Lake Van area and all 5,088 aftershocks distribution of the 23 October 2011 Van (*Mw 7.1*) and 9 November 2011 Edremit (*Mw 5.6*) earthquakes (see Table 1 for source parameters). The epicenters of the aftershocks occurred until April 2012 are plotted (Landsat/Copernicus©2016 Google, ©2016 Basarsoft). The colored dots denote the aftershock magnitudes determined by the KOERI seismic network (the inset maps) (©2018 GeoBasis-DE/BKG (© 2009), Google Maps API) and © 2018 Google Earth, Mapa GISrael, ORION-ME). The inset map (top) shows the KOERI network in E-Anatolia squared in red and stations shown by black triangles, while the inset map (bottom) shows the station locations of KOERI network in detail, together with 22 stations ID shown by red triangles, which are used for the distributional analyses of the aftershocks relocated in this study. The study area, Lake Van, is shown by blue rectangle. The catalogue-located epicenters show a compact and sigmoidal distributional pattern striking ENE (dashed red curves). The seismic density of the located hypocenters is elongated and concentrated along a landward extending sigmoidal pattern corresponding to the ruptured area, the faulting style in the lake and the location of Lake Van area (see Figure 5 for details) (NAFZ, North Anatolian Fault Zone and EAFZ, East Anatolian Fault Zone).

The October 23, 2011 Van earthquake was a somewhat unusual case concerning the anomalous occurrence and the spatial and temporal distribution of its aftershocks (M ≥ 3.5) in Lake Van (Figure 1 and Table 1). The Van earthquake was followed by numerous aftershocks with the same origin and most of the aftershock activity was restricted to a narrow area, bounded by the faults of the lake (Toker, 2017; Toker et al., 2017; Toker and Şahin, 2019); ~2,828 events occurred in the first month (November 2011), and 4,853 in the first five months (November 2011- March 2012), nearly half of which were larger than Mw 3.0. Until the end of 13 April 2012 over a period of 163 days, the total activity of 5,304 aftershocks comprised of 184 Mw ≥ 4.0 and 13 Mw ≥ 5.0 events (Bayrak et al. 2013; Toker 2014). This earthquake was associated with the local fault system aligned with the Lake Van basin that extends from west to east (Moro et al. 2014). Two weeks later, on 9 November, a second major earthquake of Mw 5.6, the Edremit event (5-7 km depths), occurred the near the southeastern coast of Lake Van along the north dipping a normal oblique-strike-slip Edremit fault (Utkucu 2013; Utkucu et al. 2013; Doğan et al. 2014) (Figure 1). This second earthquake was also associated with the local fault system (Ketin 1977; Utkucu 2006). The aftershock sequence of the November 9, 2011 Edremit earthquake worsened the situation in the area that had been affected by the previous Van earthquake. The aftershocks and the fault focal solutions of the Edremit event are on the different fault than the previous events (Figure 1 and Table 1).

Table 1. Updated source parameters of 22 earthquakes shown in Fig. 5 (compiled and modified from Irmak et al., 2012 and various institutions).

No	Date (dd/mm/yy)	Origin time (hr:mm:s)	Location (°) Lat.-Lon.	ERH (km)	ERZ (km)	Depth (km)	Mag	Strike	Dip	Rake
1	23/10/2011	10:41:21	38.7188-43.3367	3.3	1.8	15.0	7.1*	246	46	59
2	23/10/2011	20:45:34	38.6345-43.0775	2.7	0.5	5.0	5.7+	248	71	90
3	09/11/2011	19:23:34	38.4295-43.2342	2.6	0.5	5.8	5.6+	223	55	63
4	08/11/2011	22:05:50	38.7241-43.0870	0.9	0.5	4.3	5.5+	203	59	-88
5	25/10/2011	14:55:08	38.7733-43.5468	3.2	1.0	5.0	5.4+	38	41	-54
6	29/10/2011	22:42:22	38.8985-43.5503	0.9	0.2	5.0	5.3+	165	60	-56
7	23/10/2011	18:10:45	38.6980-43.3873	3.5	0.5	5.0	5.0+	289	82	35
8	23/10/2011	18:53:48	38.4072-43.3383	3.3	1.4	5.0	4.9+	219	57	25
9	23/10/2011	19:06:06	38.7868-43.2960	3.7	0.8	5.0	4.9+	228	64	-90
10	06/11/2011	02:43:12	38.9243-43.5650	1.2	0.3	5.0	4.9+	169	57	-54
11	02/11/2011	04:43:20	38.8735-43.5695	1.3	0.3	5.0	4.8+	171	58	-61
12	09/11/2011	22:38:18	38.4508-43.2085	1.9	0.7	5.0	4.5+	238	43	90
13	23/10/2011	19:43:25	38.7835-43.3447	4.1	0.9	5.0	4.4+	223	68	-90
14	24/10/2011	22:13:31	38.7710-43.1790	1.2	0.4	2.1	4.4+	183	63	-90
15	24/10/2011	18:52:16	38.7263-43.2247	1.9	0.4	2.5	4.2+	50	41	-49
16	25/10/2011	03:28:51	38.8368-43.6687	8.9	1.9	2.2	3.7+	283	57	43
17	25/10/2011	00:16:40	38.5482-43.1103	3.7	1.4	5.0	3.7+	126	74	-34
18	24/10/2011	20:15:49	38.8840-43.4742	0.9	0.3	5.0	3.6+	259	56	36
19	25/10/2011	00:26:26	38.8977-43.4658	4.0	0.9	5.0	3.6+	285	57	42
20	24/10/2011	16:24:19	38.9192-43.5143	0.4	0.1	3.7	3.6+	289	56	43
21	25/10/2011	02:39:38	38.7445-43.2055	1.3	0.5	4.0	3.5+	115	61	146
22	30/11/2011	00:47:21	38.5090-43.4058	2.6	1.2	2.8	5.0+	174	81	-32

MAG: Magnitude, **ERH:** Horizontal error, **ERZ:** Vertical error, ***Moment magnitude (*Mw*)** obtained by waveform inversion, **+Local magnitude (M_L).**

2. Literature survey

The two mainshocks of October 23 and November 9, together with thousands of events of lesser magnitude and their respective aftershock sequences, produced an intense period of intraplate seismic activity over a short time interval. This seismic activity did not appear to decrease over time and frequency, according to the known laws. The temporal propagation and evolution of the Van aftershock sequence showed a complex short and long term dynamic evolution in the aftershock area (Toker 2013; 2014; 2015). This is repeated for all the events, and may have induced alternating stress increases and decreases in either time or space, thus generating the observed clusters, declusters and dynamic complexity in the aftershock sequence (Toker 2015). If this is the case, the

rupture area of the Van mainshock ruptures repeatedly in the consecutive aftershocks and it is extremely important to reveal aftershock hypocenters of the mainshock in order to understand the focal depth nature of the rupture complexity. This suggests that the present probability of the repeated aftershock occurrence (Mw ≥ 4.0-4.5) in the mainshock area is quite high.

Soon after the Van earthquake, many geologists undertook field investigations of the surface ruptures and co-seismic deformation (Irmak et al. 2012; Koçyiğit 2012; Doğan and Karakaş 2013; Karakaş et al. 2013; Doğan et al. 2014). However, because of the occurrence of seismic-related surface ruptures, mass-wasting and landslides in the fields along the faults, the field investigations were limited to scattered sites and no information was obtained on geological nature of the ruptured area. Geophysical studies were also inadequate for determining the spatial and temporal details of the aftershock clusters around the hypocenter of the mainshock (Bayrak et al. 2013; Elliott et al. 2013; Fielding et al. 2013; Utkucu et al. 2013; Moro et al. 2014). Furthermore, the land-based observations that were conducted were insufficient to describe the overall rupture geometry and the detailed seismic activity (Altıner et al. 2013; Kalafat et al. 2013; Utkucu 2013). Prior to the present study, little was known about the focal depth nature of aftershock seismicity and structural coupling to rupture complexity at crustal depths.

Since the aftershocks following the Van and Edremit mainshocks occurred in larger numbers, they can assist in delineating the focal depth pattern of the rupture upon which the Van mainshock occurred and clarify the spatial and temporal distribution of the seismicity around the focal area. A close spatial inspection of the cluster pattern of the aftershock distribution at depths of 10 km up to 30 km implies a possible relation between the fault-controlled nucleation zone of 2011 Van earthquake aftershock sequence and P- and S-wave velocity anomalies (Toker and Şahin, 2019 and references therein). This relation seems to be due to crustal faulting movements in the Lake Van area, as explained in the tectonic model study of Toker et al. (2017) and also Toker (2017). This paper explores the structural coupling to the aftershock sequences in the Lake Van area to gain a better understanding of the hypocenter dynamics of aftershock sequence. Moreover, the current study analyzes the focal depth features of aftershocks beneath the surface based on seismic velocity observations (Toker and Şahin, 2019) and comments on rupture propagation complexity of aftershock sequence, and contributes to the investigation of the distributional configurations of the hypocenters on the scale of a few tens of kilometers. This paper presents the results of the first detailed hypocentral observations, coupled to the boundary faults of Lake Van basin, and this is important data for future seismic hazard analyses in the area.

3. Structure of Lake Van

The Lake Van region is a mantle-supported, N-S shortened domal morphological structure (Şengör et al., 2003; 2008) (Fig. 1) and presently rises above a doming, hot asthenosphere due to slab detachment and break off events in E-Anatolia (Zor et al., 2003; Zor, 2008; Şengör et al., 2003; 2008). A thin and warm crust underlies this shortened region, covered by various kinds of fluids (Turkoğlu et al., 2008; 2015), volcanic dome-cone complexes and active magmatic intrusions, typical of an extensional regime as observed in the Lake Van basin (Çukur et al., 2016; Toker et al., 2017).

The Lake Van basin is characterized by oblique-slip boundary faults; extension-transtension in E-margin, transpression in N-margin and extension-transtension in S-margin, through which magma propagation and related intrusive-extrusive occurrences are observable (Toker et al., 2017; Toker and Şahin, 2019). The oblique-slip deformation in the lake basin actively controls differential subsidence in deep basin (e.g., relaxation barrier) and differential uplift toward ENE (e.g., fragmentation barrier), where the 2011 Van earthquake occurred (Toker, 2017). Extensional-transtensional deformation observed in the lake is characterized by thick lacustrine sediments overlying a faulted layer (e.g., detachment), beneath which ductile extension may have occurred (Toker et al., 2017; Toker and Şahin, 2019). The present day deformation style of the Lake Van basin is derived from incompatibility junctions of active tectonic structures (Toker and Şahin, 2019) driven by accretionary wedges and controlled by upper crustal flake tectonics and sequential events of volcano-tectonic/magmatic processes (Toker et al., 2017; Toker and Şahin, 2019). The active deformation is within a form of fault-bounding oblique wedge, escaping toward ENE, tends to localize in, and along the weakness zones of the lake margins, where strain accumulation, condensation and partitioning, for example caused by transpression in the N-margin, are the most prominent features, as proposed by Toker et al., (2017). Tectonic mobility of this lake probably began around the Late Miocene-Early Pliocene and has intensified during the Plio-Quaternary periods (Toker et al., 2017).

4. Material and Method

The earthquake data set processed by Toker and Şahin, (2019) (catalogue published by KOERI (Boğaziçi University, Kandilli Observatory and Earthquake Research Institute) (http://www.koeri.boun.edu.tr/scripts/Sondepremler.asp/2020) were used in the present study to relocate and to plot the distribution of selected aftershocks (Figure 1). The KOERI network consists of 21 broadband and one short-period seismic stations with a sampling frequency of 50 Hz. The dynamic range is 140 and 164–184 dB for the broadband and short-period seismic stations, respectively. This network has the scheme for automatically detecting events available for processing and working with the continuous waveform data.

Toker and Şahin, (2019) performed the catalogue of KOERI to improve the data quality and to refine the depth resolution of the events given in the catalogue. This made arrival times of P- and S-waves and corresponding hypocenter locations quite reliable for seismic tomographic research reported by Toker and Şahin, (2019) and aftershock relocation analysis in this study. Hence, the current study used the routine procedures of the hypocenter location method with the Hypo71 source code and 1-D crustal velocity model derived by Toker and Şahin, (2019) for the determination of the hypocentral parameters of relocated events. (Lee and Lahr 1972), as it gives the minimum RMS travel-time residuals. Toker and Şahin, (2019) checked initial velocity models to find the best Vp/Vs ratio by using a number of slightly different initial P-wave velocity models with different Vp/Vs ratios and applied them to different sub-data sets and found a constant Vp/Vs value of about 1.778. The related cumulative wadati diagram used for initial model is constructed for this study (Figure 2), indicating that the overall seismic structure has no substantial variations, but some slight changes in the edges, suggesting the reliability of the Vp/Vs ratio in most cases (~ 1.77). Further details for data processing, inverted 3D model and inversion procedures are given through the extensive study of Toker and Şahin, (2019).

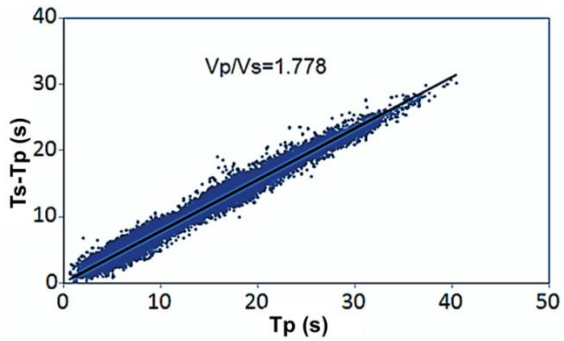

Figure 2 The cumulative wadati diagram constructed from arrival time data of our selected events provides an estimate of Vp/Vs ratio used to derive the S-wave velocity model from a known P-wave velocity model. The time difference *DT* = *Ts*-*Tp* between the arrival time of *P*-waves (*Tp*) and *S*-waves (*Ts*) was plotted against (*Tp*) for all available pairs of observations. The mean slope equaled the velocity ratio, found to be best Vp/Vs, constrained for the purpose of the optimum 1-D velocity model, based on the quality of their preliminary locations and the recording stations represented, indicating that the quality of event locations was sufficient for the purposes of the analysis in our study (derived from Toker and Şahin, 2019).

In the current study, one of sub-data sets (~ 5,000 aftershocks recorded at 22 seismic stations from KOERI in Figure 1) used in the previous study was selected from the events which occurred in Lake Van region (37 – 40°N and 41 – 45°E), implying similar ray coverage patterns of both P- and S-wave data sets from Toker and Şahin, (2019). The azimuthal gaps of the selected aftershocks for each station were carefully identified; the smallest gap is less than ~5° (356^o <gap< 360^o), the largest gap is ~180°. An important task here is to check the quality of the selected aftershocks to find the best relocation results by using available seismic velocity data. The Vp and Vs data sets from Toker and Şahin, (2019) have been analyzed for quality check of the selected aftershocks. Selected data in the study area are good at work enough to locate their own events accurately. Hence, sub-data set (e.g., phase picks, phase readings, azimuths and residuals) from nearby stations of KOERI network has been edited to increase the resolution, to improve the location quality and also to compare the residuals. The event locations and focal depths are well constrained due to both near and far stations (Figure 1) using careful selections of available P- and S-phase reads at the nearest stations to get a reliable solution and to select high-quality events and the focal depths. All residuals are stepwise examined and residuals more than the limit ±1 s are excluded from the inversion. The travel time reading errors are averaged ± 0.03 s for P-wave, ± 0.04 s for S-wave. P- and S-wave residuals are evaluated as a function of epicentral distance shown in Figure 3. Also, the initial and final RMS travel time residuals for the P- and S-wave data sets are computed as shown in Figure 4. The sum of squared travel-time residuals is reduced by more than 35% of its initial value after the inversion process. The final RMS travel time residuals were 0.33 s and 0.34 s for the P- and S-wave data sets, respectively (Figure 4).

In this study, the use of a 1-D initial velocity model of Toker and Şahin, (2019) to relocate the focal depths of selected events minimizes the relative location uncertainties by controlling the accuracy of the relative arrival-time readings with available phases and/or selecting the high-quality events and the focal depths and improves the location accuracy of data (e.g., systematic biases introduced by 3-D velocity variations). In addition to reduced residuals, epicenter locations are also evaluated according to the faults observed from seismic reflection profiles (Toker and Şengör, 2011; Çukur et al., 2013; Çukur et al., 2016; Toker et al., 2017; Toker, 2017) that can ensure reasonable depths.

In the present study, focal depth locations reveal a focused geometric picture of distributed aftershock seismicity (Toker, 2013; 2014; 2015; Toker and Şahin, 2019). Most of the aftershocks align in upper crustal depths along curve-linear, linear, horizontal streaks. Most of the aftershock activity consists of clustered similar and/or same-sized events, suggesting strong self-similarity of coupled events at depths with focal depth location errors typically about 1-2 km. Some selected events of the aftershock activity constrained by relocated catalog picks are also compared with the data set performed by previous studies (Gülen et al. 2002; Irmak et al., 2012; Bayrak et al. 2013; Fielding et al. 2013; Kalafat et al., 2013; Toker 2013; Toker 2014). The comparison indicates that overall geometric pattern of the individual events reveal the same relocated seismicity structure of Irmak et al., (2012) based on the same KOERI data set with focal depth uncertainties of 1-2 km (Irmak et al., 2012) and 2-3 km (Bayrak et al., 2013; Kalafat et al., 2013). Considering that the structure is highly complex, and based on the relocations given in this study and also the data set performed by previous studies, this study proposes a focal depth location uncertainty of ~1-2 km.

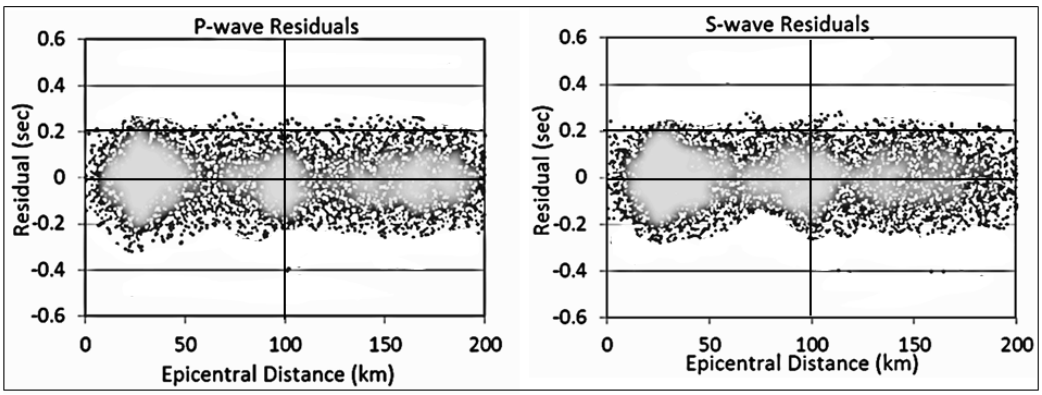

Figure 3. P- and S-wave travel-time residuals as a function of epicentral distance (offset) for the initial 1D model used in this study.

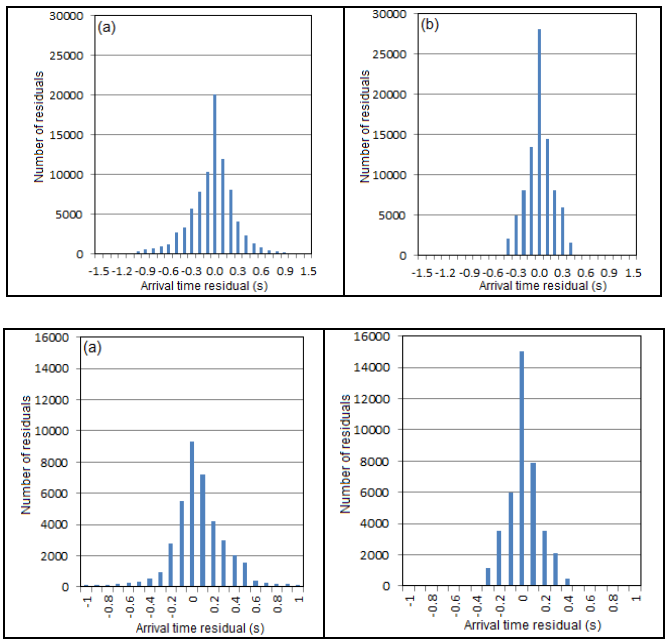

Figure 4. P- and S-wave travel-time residual histograms for both the initial 1D and the final 3D model, showing distribution of relative arrival time residuals associated with the initial model (before inversion at left column) and solution model (after inversion at right column) for P- (at upper line) and S-(at lower line) waves. After the inversion process RMS values are determined as 0.33 s and 0.34 s for the P-wave and S-wave data sets, respectively.

5. Results

5.1. Relocations associated with velocity structure

The map view of the seismic density of the relocated aftershock hypocenters includes 5,088 events shown in Figure 5. The relocation results of the selected high-quality events show that the seismicity has a maximum depth of ~30 km with peak activities at 8 and 10 km (Toker and Şahin, 2019). In Figure 5, the relocated aftershocks more than about 65 % occur below ~10 km and indicate a focused view of the cluster seismicity at ~8-10 km, compared to the more scattered locations in Figure 1.

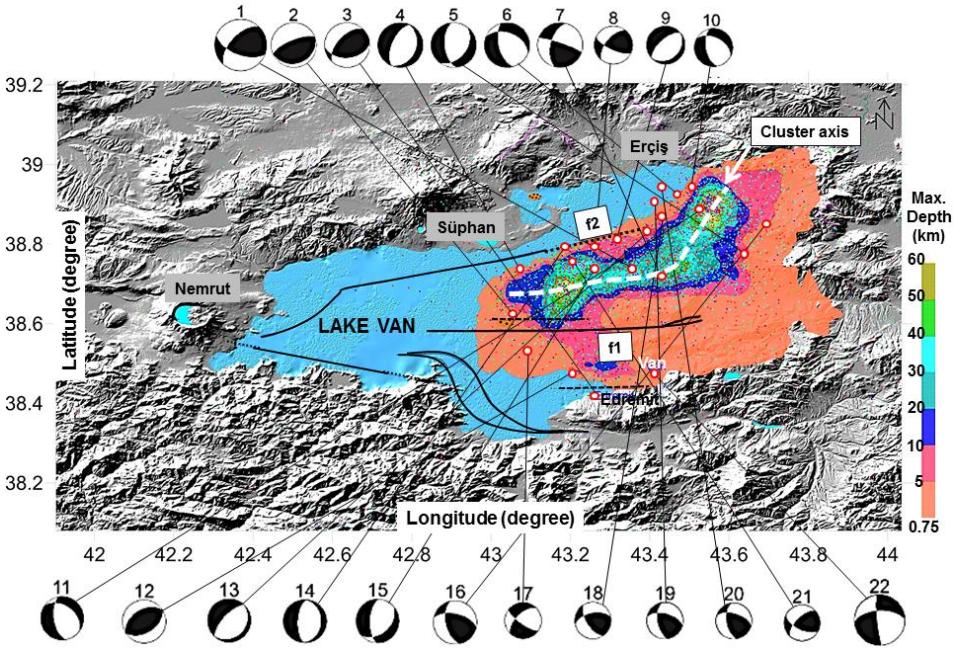

Figure 5. Shaded relief map of the focal depth distribution of the relocated aftershock hypocenters (5088 events) shown in Figure 1 in the ruptured area (map modified from Toker and Şahin, 2019). The Lake Van boundary faults (black lines) used to constrain the focal depth data are also shown (data compiled from Toker 2011; Toker and Şengör 2011; Çukur et al. 2013; Çukur et al. 2016; Toker et al., 2017; Toker, 2017). The map shows aftershock relocations, the fault plane solutions of the Van and Edremit mainshocks (numbers 1 and 3) and 20 aftershocks (white dots) of the Van earthquake with the hypocenter depths occurring during the earthquake (see Table 1 for source parameters of focal solutions updated and compiled from Irmak et al. 2012 and various institutions) (Bayrak et al. 2013; Toker 2013; Toker 2014). The numbers on the focal mechanisms indicate these aftershocks listed in Table 1. Local faults (f1, f2) are the landward continuations of basin-bounding faults in Lake Van (see tectonic and seismic b-value models by Toker et al., 2017 and Toker, 2017, respectively). The map indicates the relation of the faulting styles of the lake to the distributional density of the hypocenters (contours are depths in km, the dots denote the aftershock epicenters and dashed white line is common cluster axis). The map also indicates that seismic density of the located hypocenters is concentrated along a landward extending sigmoidal pattern corresponding to the ruptured area and the faulting style in the lake. The normal and thrust focal solutions seen are related to the rupturing of the secondary faults as a result of the rupturing of a main thrust fault plane in the NE direction and with a 58^{o}NW dip (Irmak et al. 2012). The rupturing caused secondary intra-plate deformations obtained from the fault plane solutions of the aftershocks numbered 22 on map and fits with the direction of the aftershock pattern (see focal data shown in Table 1).

Here, we conduct a spatial pattern analysis to address the distribution of the aftershock seismicity with respect to the basin-bounding faults (Figure 5). The relocated aftershocks collapse into fault-bounding discrete zone within the Lake Van area (Figure 5), and roughly follow the local zones of increased strains associated with the faults, while other located events became more spread out. Also, more aftershocks are densely positioned along the E-part of the lake, compared to the W-part. Seismic activity is increased to the E and S of the basin, while other areas remain seismically quite. When moving W in the basin along the boundary faults, the activity decreases and fades out, showing quite areas within the basin. However, the aftershock seismicity is densely distributed and clustered between the basin-bounding faults, when moving E in the basin. These observations indicate a clear "aftershock-clustered seismicity behavior" along the basin (Figure 5). This is the basic pattern of our further analyses. However, the diffuse and asymmetric distributional pattern of aftershock events associated with the low number of stations may impose a few limitations on the resolution of the observed velocity amplitudes (Toker and Şahin, 2019); the numbers of aftershock events are very sparse and the seismicity level is low in the W and central parts of the lake, while aftershocks are densely clustered in the E and NE parts of the lake.

These observations are also correlated with the multi-channel seismic reflection studies in Lake Van Basin (Çukur et al., 2013; Çukur et al., 2016; Toker et al., 2017; Toker, 2017) that indicate a tectonic mobility of cold, brittle and fragmentary crustal block (see tectonic model proposed by Toker et al., 2017 for details of upper crustal deformation). This shows the clustered behavior of relocated aftershock seismic activity that almost reaches the upper elastic crust at about 10 km (Şengör et al., 1985; Dewey et al., 1986; Şengör et al., 2008; Toker et al., 2017; Toker, 2017; Toker and Şahin, 2019) and the lower crust at about 30 km (Şengör et al., 2003; Şengör et al., 2008; Toker and Şahin, 2019). The clustered behavior of seismic activity well corresponds to the depth-dependent distributional patterns of P- and S-wave velocity anomalies given in a study of Toker and Şahin, (2019) (see Toker and Şahin, 2019 for the Vp, Vs structures and their cross-sectional profiles for depths ranging from 10 km to 30 km). The large number of data and the good ray crisscrossing in the clustered area of the lake support the reliability of the obtained velocity anomalies (Gorbatov and Kennett 2003) and their relation to the cluster.

The relocated catalog of the Lake Van study area, spanning the period November 2011–March 2014 and contains 10,000 events over three years. The depth and magnitude of the earthquakes ranged from 5 to 30 km and Mw 1.5–7.1, respectively. The relocated seismicity map of the Van mainshock-aftershock sequence for magnitudes ($Mw \geq 3.5$) is well constrained by the previously mapped faults in Lake Van Basin (Çukur et al., 2013; Çukur et al., 2016; Toker et al., 2017; Toker, 2017), showing a sigmoidal pattern of aftershock distribution and the rupture zone parallel to the Lake Van tectonic trend and approximately 60-65 km in length (Figure 5). During the period 23 October, 2011 through November 2011 to December 2, 2011, the Van aftershock sequence consists of about 3100 events of ($3.5 \leq Mw \leq 6.0$) and the recorded events of magnitude $Mw \geq 4.0$ were more than 100 occurred towards the north-east and south-west parts of the rupture area (Bayrak et al., 2013). These short-term records suggest that the seismic energy is mostly released in the form of moderate size aftershocks in the rupture area where large size asperities were found (Irmak et al. 2012; Bayrak et al. 2013).

In this study, ~150 days of aftershock data (from November 2011 to March 2012) were processed and projected from the catalogue. As a result, 4,853 aftershock hypocenters, of which 2,476 had a local magnitude greater than 3.5, were retrieved (Figures 6 and 7). In Figure 8, the cross-sections show the migrational patterns of the relocated hypocenter activity over the four periods including 4853 events of March 2012 as shown in Figure 6b. In Figure 9, the cross-section is correlated to the local faults to show a complete clusteral picture of the relocated hypocenter activity including 4853 events of March 2012 as shown in Figure 6b. Then, to establish azimuth-dependent cross-sectional images of the aftershock distribution, the epicentral distribution of 10,000 events were selected for a time period from November 2011 to March 2014 (Figure 10). Finally, to plot the temporal distribution of the aftershocks and detect the temporal and spatial clustering of microseismicity, 6,135 events were selected from 282 days covering the period from October 23, 2011 to August 1, 2012 (Figures 11 and 12). Considering Vp, Vs anomalies and their relation to the structural pattern of the cluster revealed by Toker and Şahin, (2019), generally, low Vp and Vs anomalies slightly changed to high Vp and Vs at cluster depths and were densely concentrated within the cluster at which the seismic activity was very intense with low V or low to high V.

5.2. Pattern recognition

The spatial and temporal patterns of the aftershock distribution associated with the observed clusters show no distinct difference between the periods of November 2011-March 2012 (Figures 6-9) and November 2011-March 2014 (Figure 10). The main difference is only related to the growing, tightening and deepening patterns of the observed clusters, showing a concentrated pattern of distribution and tightness of the relocated hypocenters. The hypocenter locations were compared to investigate the spatial and temporal variation of the seismicity in the clusters. The plotted hypocenter locations are closely and tightly spaced and clustered with the located clusters being densely concentrated. Also, the distributions of Vp and Vs were recovered down to crustal depths at which the cluster was observed. Tomographic imaging of the P-wave velocity structure beneath the cluster at depths of 4, 7, 14, and 23 km and the S-wave velocity structure at a depth of 14 km performed by Toker and Şahin, (2019) indicates velocity-dependent structural pattern of the cluster. This suggests that the velocity anomalies from the inverted P- and S-waves can be considered to be reliable within and nearby the cluster at depths of ~10 km up to ~30 km (the lower depth limit of seismicity in the main cluster at ~10 km in Figures 7-9 and at ~30 km in Figure 10). In the cross sections, the observed clusters concentrated within highly distinct spatial activity are also well constrained by the mapped basin-bounding faults (Fig. 5) (Toker and Şahin, 2019) and caused by subsurface stress perturbations closely occurred at similar and smaller spatial scales (Toker 2014; 2015). As a result, the pattern recognition of the clusters observed from aftershock relocation analyses is mainly based on the events concentration within highly distinct spatial activity and Vp, Vs anomalies (Toker and Şahin, 2019).

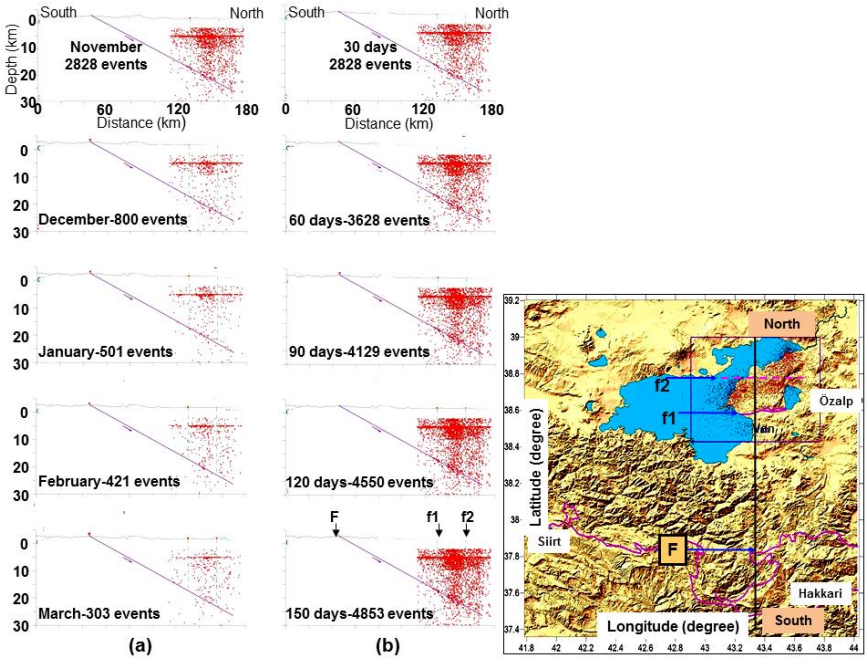

Figure 6. Distance versus depth plots of relocated distribution of all 4,853 aftershocks of the Van mainshock, for one month intervals from November 2011 to March 2012. The solid line labeled N–S in the map indicates the central line of the given cross-sections, and the solid square marks the 70-km-wide zone projected onto the cross-sections. Aftershocks within the squared area from the central line of the cross-section are projected onto the plane of the cross-section with the projected distance of 180 km. The red horizontal lineament of hypocenters refers to fixed hypocentral artefact. **a** Omori's law of decay of aftershocks identified as changing the aftershock events for each month over a five-month period are represented in their corresponding time windows. **b** Distance versus depth plots of distribution of the aftershocks within the time period from November 2011 to March 2012, with the cumulative numbers of the events for each month and the same representation criteria as in Figure 6a. F: the major regional thrust fault, f1: local thrust fault (Emre et al. 2011), f2: inferred local fault, local faults (f1, f2) are the landward continuations of basin-bounding faults in Lake Van (see tectonic model by Toker et al., 2017).

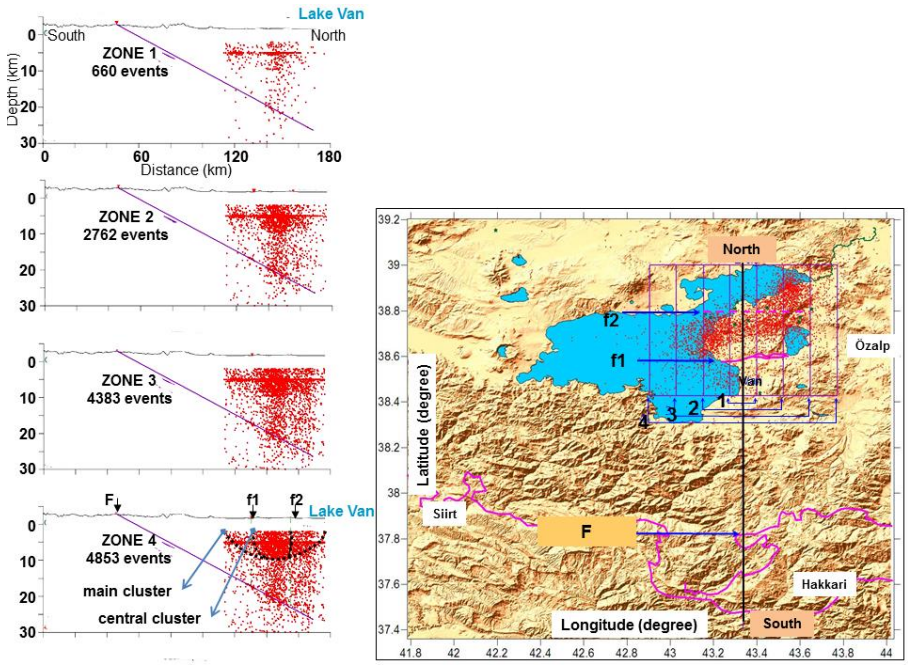

Figure 7. Relocated distribution of all the 4,853 aftershocks along four vertical cross-sections, with a projected distance of 180 km. The aftershocks are presented as the areal distributions from narrow to wide zones as shown in the map. The solid rectangles labeled 1, 2, 3, and 4 indicate the W-E extending zones from the central line of the cross-sections, and the solid square marks the 70-km-wide zone projected onto the cross-sections. Aftershocks within the different zones from the central line of the cross-section are projected onto the plane of the cross-section. The locations of the cross-sections and the areas within the projected distances are also shown. The red horizontal lineament of hypocenters refers to fixed hypocentral artefact. Zones 1, 2, 3, and 4 contain 660 events, 2,762, 4,383, and 4,853, respectively. The distributional pattern of aftershocks in zone 4 is the same as for March 2012 in Figure 6b. F: the major regional thrust fault, f1: local thrust fault (Emre et al. 2011), f2: inferred local fault, local faults (f1, f2) are the landward continuations of basin-bounding faults in Lake Van (see tectonic model by Toker et al., 2017).

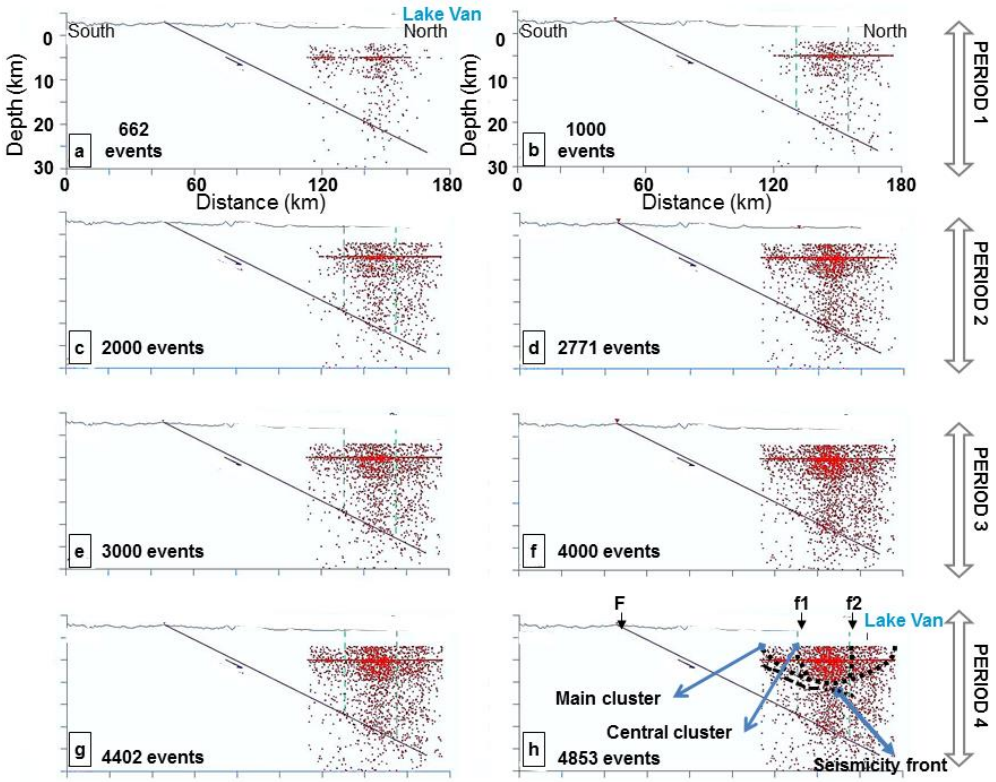

Figure 8. Relocated distribution of all the 4,853 aftershocks along eight vertical cross-sections, with a projected distance of 180 km. The red horizontal lineament of hypocenters refers to fixed hypocentral artefact. The hypocenter distribution of the aftershocks is subdivided into the four periods. Aftershocks within the area from the central line of the cross-section shown in Figure 6b are projected onto the plane of the cross-section, for each of the four periodic distributions. Each period shows the evolutionary distribution of the central and main clusters from periods 1 to 4 (see text for details). The distributional pattern of aftershocks in the fourth period is the same as in March 2012 in Figure 6b and zone 4 in Figure 7. F: the major regional thrust fault, f1: local thrust fault (Emre et al. 2011), f2: inferred local fault, local faults (f1, f2) are the landward continuations of basin-bounding faults in Lake Van (see tectonic model by Toker et al., 2017).

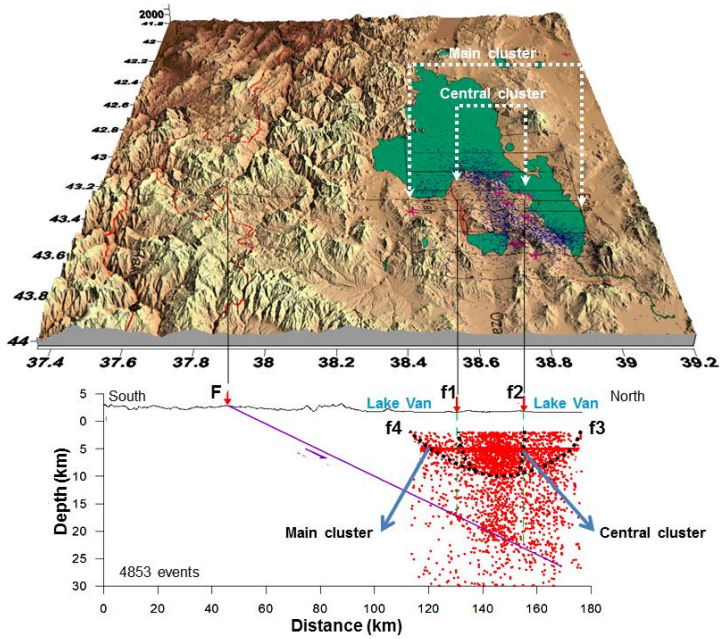

Figure 9. Relocated distribution of 4,853 events from all 5,088 epicenters in the shaded relief map along the vertical cross-section, with projected distance of 180 km. Aftershocks within the area from the central line of the cross-section are projected onto the plane of the cross-section. The red horizontal lineament of hypocenters refers to fixed hypocentral artefact. The distributional patterns of aftershocks and the clusters are the same as in the fourth period in Figure 8. F: the major regional thrust fault, f1: local thrust fault (Emre et al. 2011), f2: inferred local fault, f3 and f4: inferred local thrust faults, local faults (f1, f2) are the landward continuations of basin-bounding faults in Lake Van (see tectonic model by Toker et al., 2017).

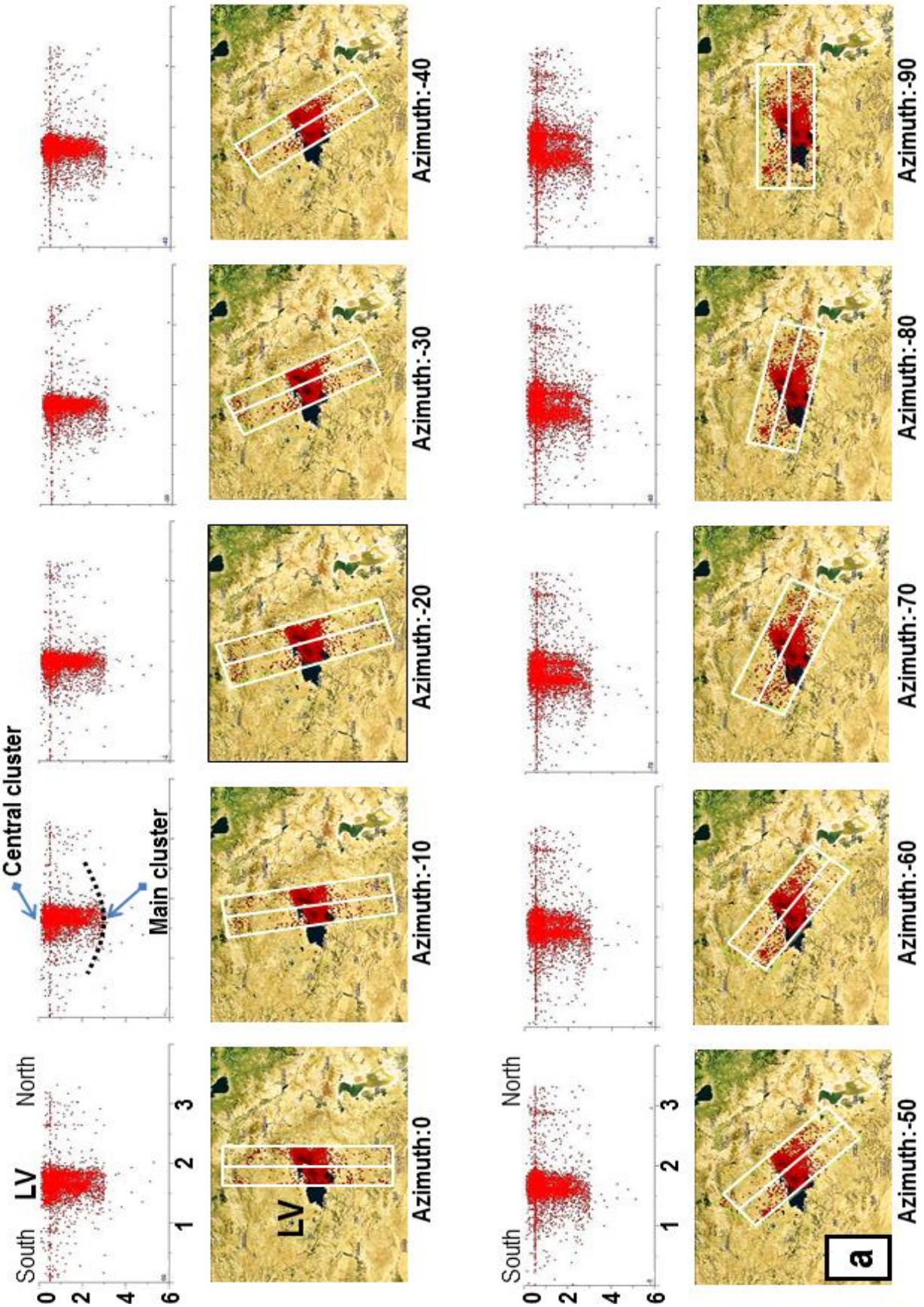
Central cluster
Main cluster
South
LV
North
0
2
4
6
1
2
3
LV
Azimuth:0
Azimuth:-10
Azimuth:-20
Azimuth:-30
Azimuth:-40
Azimuth:-50
Azimuth:-60
Azimuth:-70
Azimuth:-80
Azimuth:-90
a

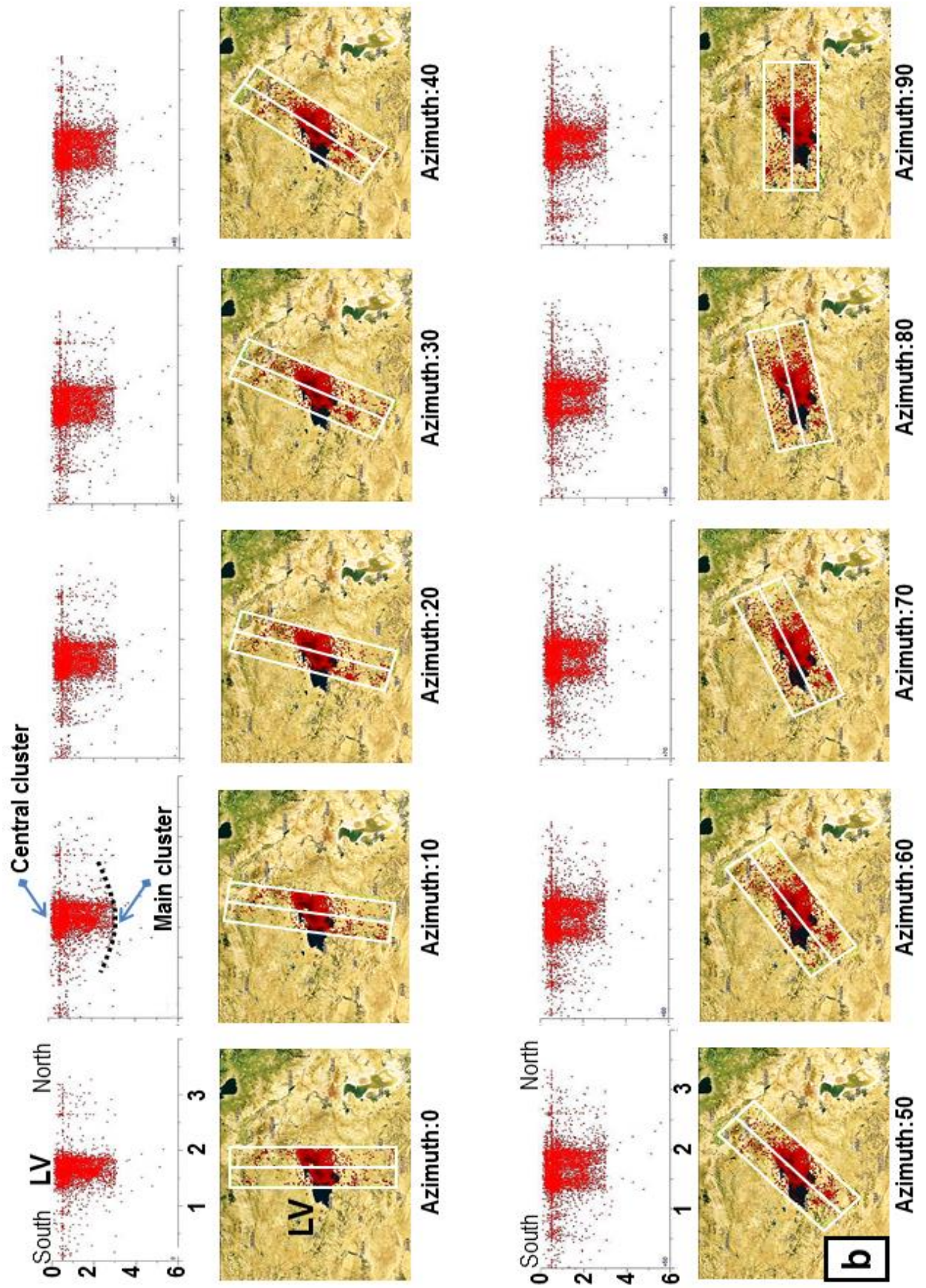

Figure 10. a. Azimuth-dependent, counterclockwise (-0° to -90°), and **b**. clockwise (+0° to +90°) distribution of all 10,000 aftershocks (November 2011-March 2014) along ten vertical cross-sections, with projected distances of 300 km (vertical axis is depth, x10 km and horizontal axis is distance, x100 km). Aftershocks (red dots) within the rectangle analysis window (white color) (1.0° x 3.0°-wide zone) from the central line of the cross-section are projected onto the plane of the cross-section and presented as a function of azimuths for each cross-sectional profile. The locations of the cross-sections and the area within the projected distance of 70 km are also shown. LV: Lake Van.

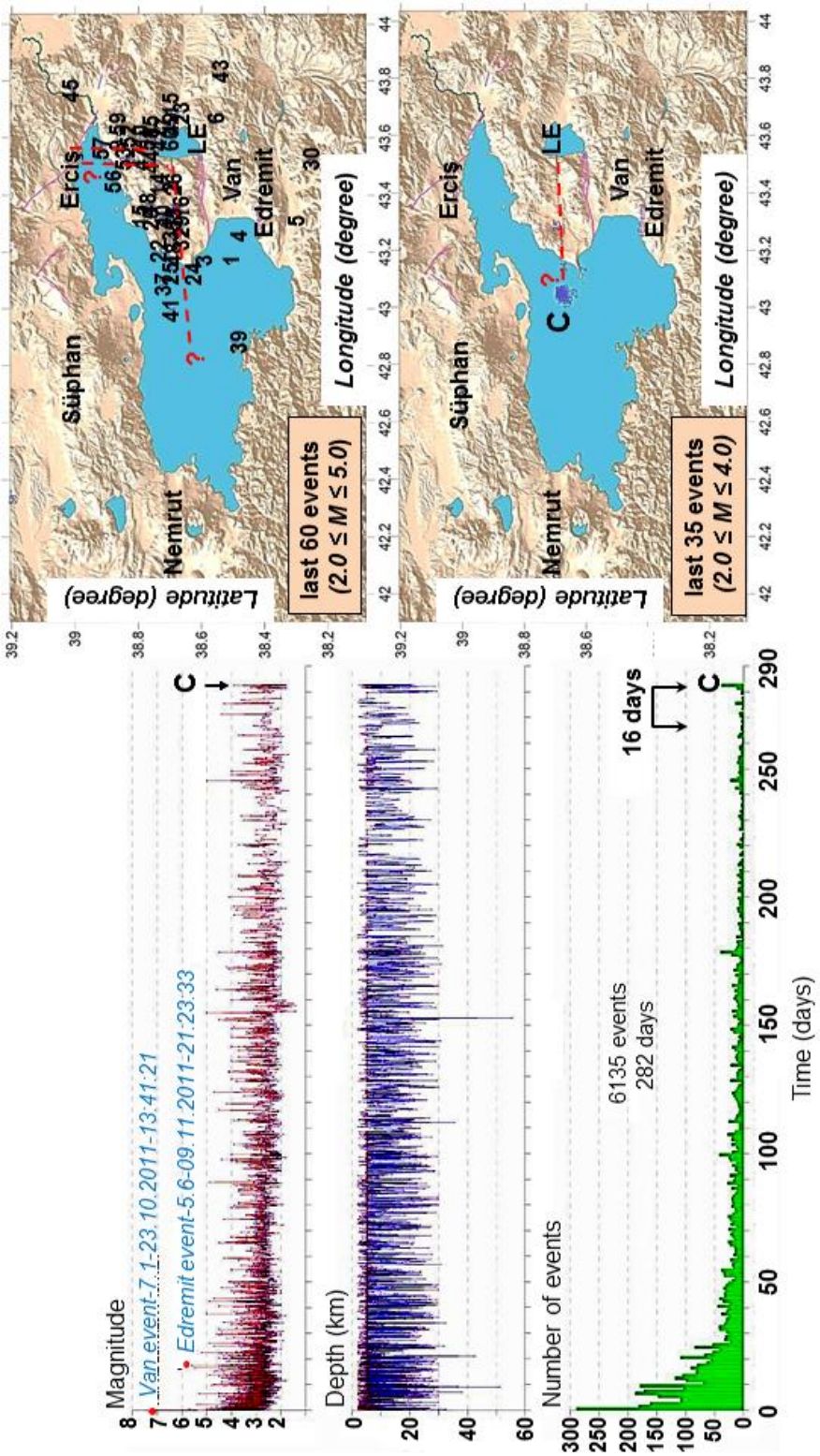

Figure 11. Temporal distributional pattern of 6,135 aftershocks from 23 October 2011 to 1 August 2012 over 282 days with the daily seismicity rate (number of events/day), focal depths (km) and magnitudes along the rupture area. A high number of events compared to the background seismicity can be seen for particular time periods indicating the temporal clustering of earthquakes along the rupture area (see Toker 2013; 2014; 2015 for temporal clusters over the whole data). Cumulative magnitudes of aftershock distribution do not exceed the commonly observed maximum magnitudes despite the very high number of events for 282 days. The last 60 events (2.0 ≤ Mw ≤ 5.0) during the last 16 days mark the most prominent sequence detected, while this sequence indicates west-east and north-south trending inferred faults and related morphologies along the rupture area (dashed red lines with question marks). On the map (top), these 60 events are relocated in numerical order according to the time of occurrence. The second prominent sequence marks the microseismicity cluster (C) also detected, containing the largest number (35 events) of the last events (2.0 ≤ Mw ≤ 4.0) indicating the spatial pattern of events cluster in the map. On the map (bottom), these 35 events are relocated in numerical order according to the time of occurrence. The map confirms the close spatial proximity of the microseismic events within the temporal cluster. LE: Lake Erçek.

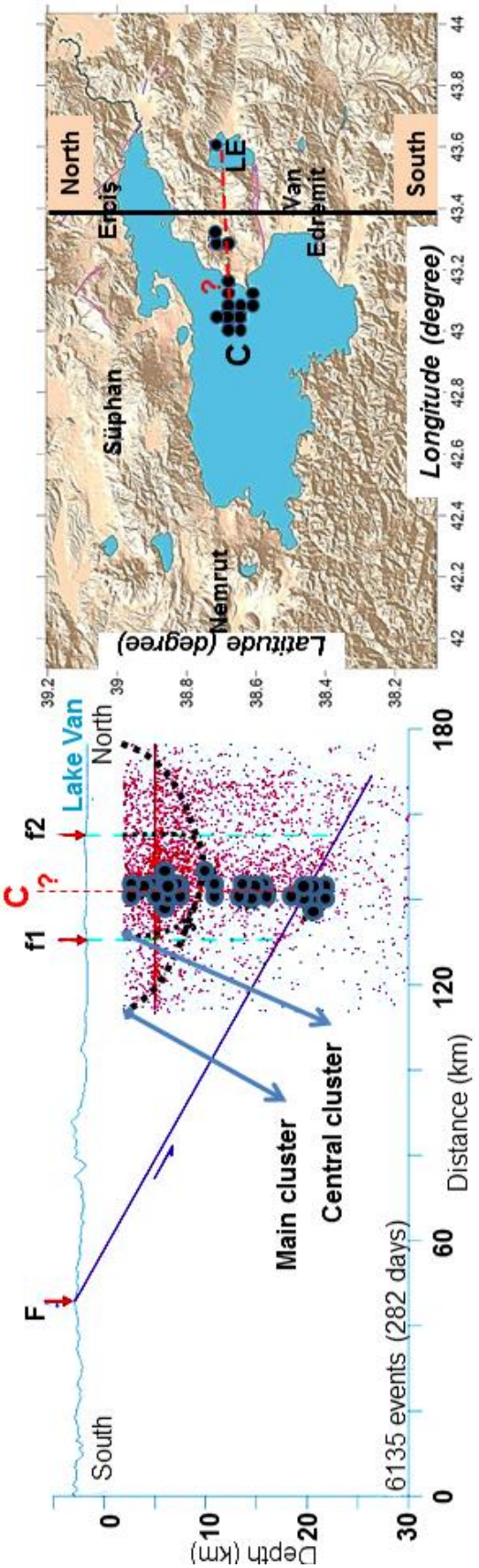

Figure 12. S-N trending, depth cross-section of the microseismicity cluster (C) shown in Figure 11 indicates the vertical hypocentral distribution (black dots) with a dip angle of ~90°. The red horizontal lineament of hypocenters refers to fixed hypocentral artefact. The map shows the spatial distribution of C consisting of 35 relocated events (black dots) (also see C in Figure 11 for location). Most events of the cluster occurred on a possible secondary fault (splay fault) close to the inferred fault (dashed red line) between f1 and f2 (central cluster). F: the major regional thrust fault, f1: local thrust fault (Emre et al., 2011), f2: inferred local fault, local faults (f1, f2) are the landward continuations of basin-bounding faults in Lake Van (see tectonic model by Toker et al., 2017), LE: Lake Erçek.

6. Interpretation

6.1. Spatial and temporal character of the 23 October 2011 aftershock sequence

This section focuses on the spatial and temporal pattern of hypocenter distribution of the October 23, 2011 Van mainshock-aftershock events, being the largest shocks of that year in the region, and on the spatial and temporal characteristics of its aftershock sequence. This section aims to shed light on the focal depth nature of aftershock seismicity and the rupture complexity of the Van event.

6.1.1 Spatial and temporal distribution of aftershock hypocenters

The map depicted in Figure 5 shows the total distribution of 5088 aftershock events used in the first step of this study. Figure 5 is also the map view of seismic density of hypocenter distribution of the Van and Edremit aftershock sequences. That figure shows the sigmoid-like propagation of the rupture area corresponding to the aftershock sequences of the Van and Edremit mainshocks, with the boundary faults located around the epicenters of Van and Edremit events. The purpose of this sub-section is simply to identify the cross-sections of the aftershock hypocenters associated with the map view given in Figure 5. To obtain a spatial and temporal overview of the seismicity pattern, the focal depth distribution of the aftershock hypocenters was examined month by month within the time period of November 2011 to March 2012. The results are presented in Figures 6a and 6b.

During the first month following the October 23 Van earthquake, different and various-sized clusters of local events occurred in the focal area (Figure 6). These aftershocks can be seen to have been gradually decaying over the subsequent months in the period up to March 2012 according to Omori's law (Omori 1884), and were dying out when the second Edremit event occurred (Figure 6a). In December 2011, the second month, the overall activity decreased continuing to decrease in the third and fourth months, and virtually ceased in the fifth month reaching 303 events (Figure 6a). In the same time period, November 2011 to March 2012, the total cumulative numbers of the aftershock activity increased (Figure 6b). Figure 6a shows that activity began to subside in March 2012, even though until the end of the July, 2012 there were several more events of $M \geq 4.0$ (Toker, 2014). The hypocentral superposition of aftershock events produced unusual seismic activity during the two last months of 2011 (Figure 6b). It appears that the Van earthquake repeatedly triggered one or more local faults in the area, and these faults in turn affected the seismicity.

In order to obtain more information from the distribution of hypocenters shown in Figure 6b to see and clarify the spatial patterns of the events distribution in detail different orientations of the focal area were tested, centering on the aftershock cloud, according to the focal mechanism given in Figure 5. The north-south trending zonal projections on the distribution of hypocenters associated with the Van event, starting with the west-east trending zonal distribution of the aftershocks for the four zones are shown in Figure 7. In this figure, the hypocenter distribution for each zone from narrow (zone 1) to wide (zone 4) indicates the first appearance of the small-sized linear clusters (zone 1) and uneven rapid concentration and densification of the event clusters (zone 2). Then, the hypocenter distribution defines a tightly consolidated and spherical (or semi-spherical) and/or parabolic pattern of the distribution (zones 3 and 4), which agrees with the distributional pattern given in Figure 6b.

6.2. The focal depth distribution of aftershock clusters

In Figure 7, the hypocenters of the aftershocks form a wide 'U' letter shaped cluster (hereafter referred to as the "main cluster"). This main cluster is a half cylinder-like channel-shaped cluster located at a broadly widening (about 60 km wide) area. The main cluster has a central (and/or core) cluster that is more tightly densified. The central cluster is narrow (about 25-30 km wide) bounded by faults f1 and f2 (Figure 5) at south and north, respectively (Figure 7). The two arms of the 'U' are symmetrically dip towards each other and are of almost the same length, about 20-30 km. The mainshock is included in the central part of the main and central cluster. The hypocenters belonging to the main cluster and its surrounding area have spans of about 25 and 30 km in the strike and dip direction, concentrated well into a depth of 8-10 km. Also, the hypocenters in the southern and northern part of the main cluster seem to be located along the extension of the plane of the central cluster aftershocks down to a depth of about 8-10 km.

The distributional pattern of hypocenters at the central cluster is fault-bounded (f1 and f2) (Fig. 5) and shows strong concentration in and around the focal area (Figure 7). However, the hypocenter activity outside the main cluster area deep down is more diffuse and few evident clusters can be seen. It is difficult to image the overall shape of the hypocenter distribution at a depth of more than 10 km due to the diffused and scattered focal depth distribution and do not seem to form a systematic pattern of the hypocenter geometry (Figure 7). The aftershocks on the periphery of the rupture area (zones 3 and 4 in Figure 7) show a more diffused distribution partly due to

the off plane aftershock activity. The location of the plane of the aftershock distribution corresponds to the upper crustal seismicity. This location seems to be a good fit with the eastward and westward limit of the in-plane aftershock activity. The zonal correlation of the events distribution from narrow (zone 1) to wide (zone 4) given in Figure 7 suggests that the shape of the upper crustal block controls the spatial extent of the asperity complex of the Van earthquake.

6.3. Migration of hypocenter activity

As shown in Figures 6 and 7, the spatial and temporal distribution of the aftershock seismicity can be explained through distinct cluster formations. The spatial and temporal variation of seismic activity is densely complex and highly clustered, comprising a repeated formation of small and large-sized clusters over brief time periods.

To further investigate the spatial and temporal variation of hypocenter activity in the main and central clusters shown in Figure 7 the hypocentral data was divided into four periods and different numbers of events for each period were used to reveal the migration and propagation of the hypocenter activity. Figure 8 displays the hypocenter activity of the March 2012 shown in Figure 6b and the distance versus depth plots for the four time periods are shown in each figure. The four periods shown in Figure 8 indicate the positions of the hypocenter activity including 662, 1.000, 2.000, 2.771, 3.000, 4.000, 4.402, and 4.853 events, respectively. Figure 8 reveals that the seismic activity began near the peripheral parts of the main cluster with small-sized linear clusters (a) and then migrated to the center and the north and formed the first traces of the central and main clusters (b) during the first period. The activity in the northern part started to accumulate in the center (c) and then, the activity jumped to the south during the second period. In the south, many aftershock events occurred, particularly larger events with magnitudes greater than 3.5 and the central and main clusters were apparently formed (d). During the third (f and e) and fourth periods (g and h), the hypocenters were distributed across entire clusters. Thus, the central and main clusters were tightly consolidated. In Figure 8, the lower bound (seismicity front) of the main cluster increases over time, rapidly in the second period and this change in depth reaches 10-13 km. This parabolic-like envelope of the main cluster characterizes the diffusion-like front migration (g and h).

In the cross sections, the shallow and deep migration of hypocenter activity in the main and central clusters is shown in Figure 8. The hypocenters of more than 10 km seem to penetrate the deeper levels and those shallower than 10 km are located in the main and central clusters. The diffusivity is smaller inside the clusters and larger outside and towards the deeper levels. It can be inferred from the distance versus depth plots in Figure 8 that the migration and diffusivity of the hypocenter activity seems to increase over time from November 2011to March 2012, with the maximum diffusivity recorded in November 2011, when the seismic activity had increased drastically (2,828 events shown in Figure 6b). The general periodic trend of the migration of hypocenters and diffusivity implies that the aftershock activity accelerated during the second period of seismic activity for event numbers 2,000-2,771 (Figure 8). In Figure 8, the migrational pattern of hypocenter activity indicates spatially predominantly linear to planar hypocenter distributions in the first period, but quickly changes to parabolic and then to spherical (periods 2 and 3), and a more spherical spatial pattern in the last period. This suggests that the hypocentral variation of seismicity is not unidirectional but very complex.

To interpret the main and central clusters, the hypocenters of the 4,853 events are projected on the epicenters of the 5,088 events shown in Figure 9. The aftershock hypocenters are mainly distributed in the central section of the focal area. The main cluster is interpreted to be limited by the possible reverse faults f4 and f3 in south and north, respectively, while the central cluster is bounded by faults f1 and f2 (Fig. 5). This suggests that the distributional pattern of the main and central clusters in the rupture area appears to be separated by fault-bounded crustal blocks (Fig. 5), which are initially proposed by Toker et al., (2017) and well constrained by Toker, (2017) based on the Gutenberg-Richter seismic b-values (Gutenberg and Richter, 1944).

6.4. The Azimuth-dependent distribution of seismic activity

The spatial and temporal distributional patterns of the aftershock hypocenters were noted in the previous sections. To investigate their seismic activity in greater detail, approximately 10,000 events were recorded in the time period from November 2011 to March 2014 (Figure 10). The epicenters and hypocenters were replotted using a rectangular-shaped analyse window (1.0^o x 3.0^o) to observe the azimuth-dependent changes of the aftershock seismicity projected on the distance versus depth plots. This is a very useful tool for investigating the hypocenters of events in the main and central clusters and their focal depth changes. Since the distribution of the seismic activity strongly depends on the azimuth and azimuthal rotation, and the aftershock events located within the mainshock area are considered to be representative. For comparison, the aftershocks are shown using the azimuth-dependent projections.

Counterclockwise (-) and clockwise (+) rotational projections were applied to the events with rectangular-shaped analysis window of 1.0° x 3.0°. Hence, the azimuth-dependent rotation of the depth versus distance plots were used with varying rotation angles. The azimuth is 0° for the projections trending north-south, and ranges from -10° to -90°, for the counterclockwise rotation shown in Figure 10a and from +10° to +90° for the clockwise rotation given in Figure 10b, respectively. Then, the azimuth-dependent changes of the events are projected on the depth versus distance plots and shown along the lines of ten cross-sections (Figure 10).

The overall aftershock distribution on the cross-sections shown in Figure 10 roughly corresponds to the aftershock activity on those cross-sections (Figures 6-9). Along the azimuth-dependent projections, it can be seen that most of the hypocenter activity densely occurs just beneath the mainshock area and the central and main clusters are combined into the one unique and larger cluster at a depth of 30 km (Toker and Şahin, 2019). The cluster on the projections with an azimuth of 0°-40° and -50°-90° seems to have conical-shaped narrow and wide volumetric patterns, respectively (Figure 10a). These conical-shaped volumetric patterns of cluster seem to have the square-like widening patterns (Figure 10b). This suggests that the hypocenter activity migrates, extends down to ~25 km, with the maximum depth being 30 km and covers the whole crustal seismicity (Toker and Şahin, 2019). Given that the average cutoff depth of ~30 km represents the seismic base of the crust along the rupture fault system, the seismicity distribution indicates that the upper crust in the study area is brittle and seismogenic, and that the brittle–ductile transition may occur at the transition between the middle and upper crust. Since most of the aftershocks were found beneath the surface outcrops of the focal area and the basinal area of Lake Van with sparse aftershocks may represent the base of the thick sediment body.

The cross-section shown in Figure 9 is oriented south to north with 0° azimuth (see Figure 10). The hypocenters depicted on this cross-section show a possible convergence at depths of ~8-10 km. The projection of the central cluster onto the plane of the cross-section is located around the mainshock surface rupture in the narrow area between Lake Van and Lake Erçek (faults f1 and f2 in Figure 9). Therefore, currently the central cluster is highly active and considered to represent the deep rupture associated with the mainshock and the main cluster appears to have been activated by the pre-existing low-angle reverse faults (f3 and f4). The cluster distribution suggests that the upper crust is so inhomogeneous and complex that an earthquake rupture would be an insufficient description based solely on the distributional pattern of the hypocenter.

6.5. Microseismicity clusters

This sub-section further analyzes the spatial and temporal aftershock sequences occurring along secondary and/or splay faults at or along the fault-bounded (f1 and f2) central cluster shown in Figure 9. If the central cluster is currently highly active and considered to represent the deep rupture complexity, the close spatial and temporal proximity of microseismic events need to be used to improve the visual resolution of hypocenters in the central cluster. Hence, similar events were searched for using the temporal clustering procedure (Toker 2013; 2014) to locate the clustered microseismicity occurring within small volumes. Figure 11 shows the temporal distribution of aftershocks and temporal relation of the clustered events comparable to the magnitude and the focal depth versus time plots.

The temporal distribution of the aftershocks analyzed in this study consists of a total of 6135 events over 282 days (October 23, 2011-August 1, 2012) in three different plots with Mw > 2.0 earthquakes occurring sequentially one after another with the duration of each day being less than 24 hrs (Figure 11). In Figure 11, the prominent temporal activity sequence contains 60 events ($2.0 \leq Mw \leq 5.0$) occurring within the previous 16 days, with the strongest of the temporal activity clusters including 35 events ($2.0 \leq Mw \leq 4.0$) occurring within less than 12 hrs. The last individual temporal cluster was identified and analyzed, including the last 35 events. This cluster indicates that the temporal activity of the cluster is spatially concentrated within distinct activity events (Figure 11).

As shown in Figure 11, the most prominent sequence observed along the inferred fault consists of 60 located microearthquakes all occurring within 16 days preceding 31 July 2012 and within the ruptured area between Lake Van and Lake Erçek. This sequence indicates a west-east trending morphology of the inferred fault. The observed prominent temporal cluster consisted of 35 located microearthquakes that all occurred within a time period of less than 12 hrs on 1 August 2012 and within an area of about 2.5-3.0 km^2. The epicentral alignment of the events suggests an east-west striking orientation in the map view. The strike of the aligned events with the cluster and the local trend of the ruptured area suggest a junction between the main fault branch and a splay fault at the cluster (Figure 11). For a further analysis, the hypocenters of temporal cluster were plotted on a depth section trending north–south to observe the general trend of the events as identified in Figure 11. The 35 microearthquakes are observed that all occurred at the central cluster with varying depths (Figure 12). These events are linearly aligned in the section with the activity expanding to shallower depths, the hypocentral depths of the events range from 3 to 20 km, but remain limited to a depth of 20 km, and suggest a steep dip (≈ 90°) (Figure 12). The events were

systematically spread along the plane of the section with a gradual increase of number of events during the most active part of the cluster. The largest event occurs with Mw 4.0 and the centroid of the activity then migrates to the central cluster bounded by faults f1 and f2 (Figure 12). The hypocenters define the starting point of the cluster followed by a systematic migration throughout the central and main clusters shown in Figure 9.

The linear distributional pattern of the events cluster suggests vertical migration of the aftershock activity and most probably indicates the nucleation point of the failure between f1 and f2 and the progressive failure of adjacent patches of the possible fault (Figure 12). This was initiated on the central cluster and propagates vertically into the possible fault. The temporal distribution of the aftershock magnitudes, focal depths and the number of events observed within the cluster increased and then gradually decreased. The events cluster observed in Figure 12 represent the complex behavior of the rupture process within the central cluster.

7. Discussion

This paper reports on a study of the structural coupling to the Van earthquake aftershock sequence with the following five aims:

(i) to identify the aftershock hypocenters and their spatial and temporal distributions linked to the mainshock and basin-bounding faults (f1 and f2) mapped from seismic reflection data in Lake Van Basin (Fig. 5) (Toker, 2011; Toker and Şengör, 2011; Çukur et al., 2013; Çukur et al., 2016; Toker et al., 2017; Toker, 2017);

(ii) to observe the aftershock clusters, their focal depth distributional patterns;

(iii) to understand the migration of the hypocenter activity associated with each observed cluster;

(iv) to determine the azimuth-dependent distribution of seismic activity; and

(v) to detect an individual temporal cluster of microseismicity along the ruptured area in the Lake Van region.

Our analysis of the aftershock sequence leads to the result that the observed hypocentral activity, the main and central clusters and their surrounding events show prominent patterns of the distribution. The seismic velocity structure of the main/central cluster as a function of depth was also imaged by tomographic inversion of the P and S waves (Toker and Şahin, 2019). In our study, the cross-sections showed a very distinct cluster pattern of the relocated events and the velocity-dependent structure of the main/central cluster at depths smaller than 30 km. The cluster activity was very intense along highly heterogeneous focal zone characterized by low to high P-wave and low S-wave velocity anomalies. The spatial extent of the rupture area was fault-controlled extending from Lake Van Basin (Fig. 5) and found to be almost the same as the size of the aftershock distribution (Figures 6-9). These correspondences suggest that the aftershock distribution obtained by this study reflects an exact hypocentral picture of the crustal profile of the 2011 Van event (Figure 9) and a strong coupling to basin-bounding faults of Lake Van.

7.1. Spatial and Temporal Character of the Aftershock Sequence

The overall pattern of the hypocenter distribution is seen to be terminated by the north- and south-trending arms of the U-shaped main cluster (Figures 7-9). This suggests that the north and south arms mark the up-dip limit of the rupture area of the mainshock. In Figure 10, the distributional pattern of the hypocenters extends more, to the deeper levels than the location of the main cluster as shown in Figures 8 and 9. This suggests that the coseismic slip distribution may be shifted compared to the previously determined hypocenter distribution. The aftershock activity may be inactive in the asperity region (e.g., the central cluster), where there is a large amount of coseismic slip (e.g., Hino et al. 2000; Scholz 2002). In the Van earthquake case, the aftershocks around the mainshock epicenter concentrated into large clusters and several areas of low seismicity may be the locations of the asperities ruptured by the mainshock (Yaginuma et al. 2005).

The northern and southern limits of the hypocenter distribution of the main cluster (Figures 7-9), which are interpreted as the northern and southern limits of the rupture area of the Van earthquake, correspond to the upper crustal-block seismicity in eastern Anatolia (see Şengör et al. 1985; Dewey et al. 1986; Şengör et al. 2008; Toker et al., 2017 for crustal flake tectonics). The rupture propagation of the Van earthquake may be terminated by possible crustal fault planes (f3 and f4) located about 8-10 km up-dip of the hypocenter (Figure 9). This termination of the rupture propagation may have been caused by the reduction of the stress at the tips of growing faults by the seismic deformation spread over a broad zone, as shown in Figure 10 (King and Nablek 1985). It can be suggested that the intraplate crustal seismicity (Toker, 2013) is activated along the west-east trending southern and

northern arms of the main and central clusters (compare Figure 9 with Figure 10) as the result of the rupture termination process.

Toker (2015) reanalyzed seismic network data to compare the distributional pattern of the 4853 aftershocks (see Figures 6-9) with the 10,000 aftershocks (Figure 10) and the background seismicity pattern (Toker 2014). This comparison indicates that the positions of the active aftershock seismicity show spatial and temporal variations. That is, the positions of hypocenters and the overall geometric patterns of the clusters show the azimuth-dependent spatial variations along the distance versus depth plots (Figure 10). This may suggest seismic coupling and its spatial variations thus, implying that this seismic coupling is strongly controlled by the persistent temporal and spatial clusteral nature of the Van event, such as structural heterogeneities, irregular strain accumulations, slip defects along or in the intraplate setting (Toker 2014; 2015). This reveals that the hypocenter distribution of the aftershock activity strongly reflects the spatial and temporal variation of the intraplate seismic coupling (Toker 2014).

The spatial and temporal clustering of microseismicity is also detected along the ruptured area in the Lake Van area (Figures 11 and 12). The hypocenter distribution of a single individual cluster represents an upward migration of microseismicity on an evolving subsidiary fault (Figure 12). The west-east trending fault morphology hosting cluster shown in Figure 11 forms part of the evolving fault network in the rupture area where the spatial and temporal distribution of the events are densely concentrated (Toker, 2017). The temporal clusters are associated with the earthquake sequences and frequently represent progressive failure of adjacent fault patches along planes of activity (Toker 2013; 2014). These clusters are interpreted to represent repeated failure on the same source patch and considered to be hosted within the complex fault structures under non-uniform stress fields (Ben-Zion 2008; Toker 2013; 2014). This indicates that the spatial and temporal pattern of the events is associated with the currently active faults that display similar kinematics throughout the ruptured area (Çukur et al., 2016; Toker et al., 2017; Toker, 2017). This consists of a complex network of fault instabilities and/or patches connecting fluid-filled extensional cracks and/or fractures (Hill 1977), assuming that the nature of seismic deformation energy released was in a discrete form of spatial and temporal distribution of the aftershocks in and around the ruptured area (Toker 2014). This offers evidence of the temporal and spatial density of microseismicity clusters under the ruptured area, associated with discrete form of events due to the presence of disordered fault zones and high fracture density in the seismogenic crust (Bayrak et al., 2013; Toker 2013; 2015; 2017).

7.2. Structural coupling to the rupture complexity of the Van earthquake

The analyses, in this paper, of the structural coupling to the Van aftershock sequence are often associated with mapped faults in the Lake Van Basin (Fig. 5) (Toker, 2011; Toker and Şengör, 2011; Çukur et al., 2013; Çukur et al., 2016; Görür et al., 2015; Özalp et al., 2016; Toker et al., 2017; Toker, 2017). The joint interpretation of aftershock sequence and seismic reflection profiles reveals the lateral and vertical heterogeneity of the fault-controlled aftershock distribution and along-strike seismic activity in crust within the rupture area. This suggests that the Van earthquake rupture process at crustal depths was not a simple frictional slip failure on the pre-existing, weak fault systems, but a more complex process that involved the fracturing of strong rock blocks (Bayrak et al., 2013; Toker, 2017). This means that the rupture area of the Van event is a fault-bounded fragmentation barrier (see Toker, 2017 for details). Such a local strong area (e.g., large asperity and/or barrier) is highly resistant to rupture growth on a fault and this area plays a more important role in determining the size of an earthquake than the remainder (e.g., aseismic slip and/or relaxation barrier as proposed by Toker, 2017) of the fault plane, which has little resistance to rupture growth (Ohnaka and Kato 2007; An et al. 2010). Moreover, hypocenters and their distributional patterns (e.g., the migration, diffusion, scattering and clusters) are also the consequence of stress redistribution related to the mainshock, occurring as failure along smaller fault asperities (Toker, 2017). Aftershocks involve lower stress values than the mainshock and thus, may occur at greater depths and over wider areas than the mainshock (Strehlau, 1986). In the present case, most of the aftershock hypocenters rapidly occurred and formed the clusters beneath the mainshock area, where the portion of the upper crust consists of the thrusted slices with volcanic materials (Şengör et al. 2003; 2008; Toker et al., 2017; Toker, 2017) and may contain asperities and barriers (Toker 2014). This may explain the spatial and temporal heterogeneity of the aftershock seismicity.

The anomalous distribution of larger aftershock activity after the Van mainshock also showed a triggered pattern of multi-clusteral events (Mw ≥ 4.0) and extreme heterogeneity of the faulting in the rupture area (Toker 2013; 2014; 2015), supported by the large size asperities in the rupture zone of the mainshock (Irmak et al. 2012; Koçyiğit 2012). The short and long-term temporal activity of distinct clusters defined by Toker (2013; 2014) permits a better understanding of the rupture process in the local-scale seismicity along the ruptured area. Thus, the epicentral pattern of sequential events and hypocenters of microseismicity clusters supply important

information by providing clues to the ruptured area (e.g., fracture, crack and permeability identification). The spatial and temporal distribution of microearthquakes and their systematic migration within individual clusters during the progressive failure of neighboring fault patches may define the simple picture of individual fault patches. Hence, the temporal pattern of seismic sequences observed in the ruptured area may suggest a progressive failure process on adjacent fault patches.

Considering the above results, the structural coupling of the Van aftershock sequence is that the 2011 Van mainshock strongly triggered later events associated with a system of crustal faults along the accretionary wedge complex of Eastern Anatolia, and at the same time some crustal faults were activated reciprocally and new events were induced in the focal area. For example, the second destructive earthquake of Mw 5.6 (Edremit event) on November 9 was located on one of these faults, which probably had sufficient accumulated energy, and the stress storage derived from the adjustment of the tractions after October 23 acted as a trigger. The Van mainshock-aftershock sequence indicates the conditions under which aftershock events may interact with the other events (e.g., Edremit aftershock sequence) to repeat or renew the interactions of events (Toker 2013, 2014). The superposition of both the mainshocks within such a short interval of time with the respective aftershock sequences produced an intense spatial and temporal period of seismic activity that did not decay according to known simple laws.

7.3. Implications for the damaged area in and around Lake Van

The structural coupling of the Van aftershock sequence associated with the mapped faults in Lake Van Basin reveals an increasing damage pattern with internal damage zones in the Lake Van area. The highly damaged rheology caused by the Van earthquake in multiple zones with a variable density of cracks/fractures/secondary smaller faults manifested as activated fields of intraplate stress heterogeneity (Toker 2013), reduced elastic moduli and increased dilatancy and anisotropy. These zones produced locally varying focal mechanisms and a high variance of the stress fields (Bayrak et al. 2013; Acarel et al., 2014; Gori et al., 2014; Toker 2014).

The post-seismic hypocentral behavior of the Van aftershock sequence also exhibits distinct patterns of clusters and anisotropy in the distribution and redistribution of stresses over space and time (Altiner et al. 2013; Toker 2013; Mackenzie et al., 2016). The damaged area from the Van event had a distinct asymmetric aftershock response to loading under heterogeneous stress conditions and clusters (also with decluster, quiescence and power-law truncation of events) during the loading-unloading intervals (Toker 2013). This was mainly due to a higher energy dissipation associated with the creation and activation of new small faults, microcracks and fractures (increasing damage) and the inelastic deformation of the internal damage zones (Ben-Zion 2008). These results imply that the asymmetry of the aftershock response to seismic deformation (damaged area) became extreme and strongly anisotropic across a wide range of size scales of the damage in the Lake Van area (Ben-Zion 2008; Toker 2013; 2014). This requires a view of the discrete framework commonly used in a statistical mechanics approach (Ben-Zion, 2008). The post-seismic hypocentral behavior of the Van aftershock sequence is, in fact, similar to the readjustment of crustal stresses (Khilyuk et al. 2000) in intraplate accretionary orogens (Şengör et al. 2003; 2008). This supports the argument that the real cause of the anomalous occurrence and distribution of aftershocks and their hypocenters may be anisotropic stress transfer and the rapid dynamic redistribution of stresses rather than the gradual static increase (Khilyuk et al. 2000; Ben-Zion 2008). This assumes a discrete structural model of the seismogenetic crust and suggests a dynamic origin of the 2011 Van mainshock-aftershock generation rather than the static concept of accumulated stresses (Toker 2014).

Previous studies of the 2011 Van event reported the heterogeneous stress and strain regimes in and around the focal area, however, they did not reveal how the seismic activity and related stress regime changed spatially and temporally. Several shallow faults observed in the field slipped for days and weeks after the mainshock. These shallower faults in the crust now have increased stress and were reported to have been triggered from the dynamic and static stress changes of the mainshock (Fielding et al. 2013). It can be postulated that spatial and temporal variations of the Van aftershock sequence, representing dynamical characteristics in the distribution of the spatial hypocenter locations of events, are related to changes in the high stress regimes. Our results show that the observed spatial and temporal variations in the seismicity are most likely due to significant changes in the local stress regime over an 3-year period, ranging from reverse-thrust faulting (fractures closing) via a strike-slip regime and finally to extensional faulting (fractures opening) (Irmak et al., 2012; Çukur et al., 2016; Toker et al., 2017; Toker, 2017). Although large scale geophysical studies surrounding the study area document seismic velocity variations in heterogeneous crust (Çınar and Alkan, 2017; Alkan et al., 2020), anomalous low resistivity through upper crustal complexity (Turkoğlu et al., 2008; 2015) and slab detachment and break off activity beneath the Lake Van area (Zor et al., 2003; Zor, 2008), the detailed origins of these changes are not clear yet however, these results are critical for forthcoming large earthquakes and seismotectonics of E-Anatolia.

8. Conclusions

This analysis of the structural coupling to the 2011 Van earthquake aftershock sequence leads to the main conclusion that the observed hypocentral activity, the main and central clusters and their surrounding events show distinct distributional patterns of the rupture complexity of aftershock sequence. The aftershock distribution and its size reflect the spatial extent of the rupture area and offer an exact hypocentral picture of the crustal profile of the 2011 Van event.

The overall distribution of hypocenters is concentrated around the mainshock hypocenter and forms two prominent clusters consisting of the central and main clusters. The main cluster bounded by possible reverse faults f4 and f3 seems to have been activated by the pre-existing low-angle reverse faults, while the central cluster bounded by faults f1 and f2 is currently highly active. The distributional pattern of both clusters in the rupture area appears to be separated by fault-bounded crustal blocks, representing the deep rupture. The migrational patterns of the hypocenter distribution indicate predominantly spatially linear to planar hypocenter distributions in the first period, but quickly change to parabolic and then to spherical, acquiring a more spherical spatial pattern in the last period. The location of the plane of aftershock distribution corresponds to the upper crustal seismicity and the zonal correlation of hypocenter distribution from narrow to wide suggests that the shape of the upper crustal block controls the spatial extent of the asperity complex of the Van earthquake. The spatial and temporal distribution of aftershock sequence with the observed clusters suggests that the hypocentral variation of seismic activity is not unidirectional but very complex and highly clustered, consisting of the repeated formation of small and large-sized clusters over brief time periods.

The most dense hypocenter activity occurs just beneath the mainshock area along the azimuth-dependent rotational projections. Only one, unique and larger cluster is observed in the projections at 30 km depth. Depending on the azimuthal rotations, the distributional pattern of this cluster ranges from the conical-shaped to the square-like narrow and widening volumetric patterns and covers the whole crustal seismicity. An individual temporal cluster of microseismicity and its spatial distribution can be observed in the rupture area. The spatial and temporal distributional pattern of each microseismicity cluster represents the vertical migration of the aftershock activity on an evolving subsidiary fault and indicates the nucleation point of the failure between faults (f1 and f2) and the progressive failure of adjacent patches of the possible fault. The west-east trending fault morphology hosting cluster forms part of the evolving fault network in the rupture area. This cluster suggests the complex faulting behavior of the rupture process both within and through the central cluster.

The results from the current study show that the observed spatial and temporal variations of the Van aftershock sequence represent dynamic characteristics in the distribution of the spatial hypocenter locations of events and related to significant changes in the local stress regime over an 3-year period. This indicates a rapid dynamic redistribution of stresses rather than their gradual static increase, suggesting the azimuth-dependent spatial variations of the intraplate seismic coupling along the distance versus the depth plots and anisotropic stress transfer through the occurring events. This study provides valuable insight into the structural interaction of the Van aftershock events at various scales comparable to, or better than the earthquake source dimensions. Hence, this analysis of the structural characteristics of the 2011 Van mainshock might a give a clue to understanding the seismogenesis in the area; however, this approach to the Van rupture complexity is still lacking in terms of various stress and strain sources. To improve our study, a promising approach is to undertake a high-resolution spatial analysis of a much larger number of different events and clusters including strike-slip aftershocks and volcano-magmatic (e.g., swarm) activities.

Acknowledgement

The author thanks all the members of the Kandilli Observatory and Earthquake Research Institute (KOERI, Turkey) for providing the continuous seismological data (DDA catalogue and Sfile documents) used in this study. The author is also grateful to; Prof. Dr. Ali Pınar (Boğaziçi University, KOERI, Turkey), Prof. Dr. Şakir Şahin (Suleyman Demirel University, Turkey), Prof. Dr. Esa Turunen, Prof. Dr. Elena Kozlovskaya (University of Oulu, Sodankylä Geophysical Observatory, Finland) for help in providing the opportunity to use the earthquake data, the depth-dependent Vp, Vs anomalies and the seismological laboratory, Prof. Dr. G. Berkan Ecevitoğlu for providing the aftershock data monitoring FORTRAN code and commenting on concluding remarks of this study. The author offers sincere thanks to Prof. Dr. Sebastian Krastel (Kiel, Germany), the leader of the Lake Van Project seismic survey, for providing the multi-channel seismic reflection profiles (International Continental Drilling Program, ICDP-PaleoVan Project-2004 funded by Deutsche Forschungsgemeinschaft collected from Lake Van basin. Also, the author offers his greatest thanks to the editors and the two anonymous reviewers for their constructive comments and suggestions which helped improve the manuscript. Some of the figures were generated by the

Generic Mapping Tools (GMT) code developed by Wessel and Smith (1998). Basemap images for the Figure 1 were produced by Landsat/Copernicus © 2016 Google, © 2016 Basarsoft, and © 2018 GeoBasis-DE/BKG (© 2009), Google Maps API and © 2018 Google Earth, Mapa GISrael, ORION-ME.

Conflict of Interest

No conflict of interest was declared by the author.

References

Acarel, D., Bulut, F., Bohnhoff, M., Kartal, R., (2014) Coseismic velocity change associated with the 2011 Van earthquake (Mw 7.1): crustal response to a major event. Geophys. Res. Lett. 41.

Alkan, H., Çınar, H., Oreshin, S., (2020) Lake Van (Southeastern Turkey) Experiment: Receiver Function Analyses of Lithospheric Structure from Teleseismic Observations, Pure and Applied Geophysics, doi:10.1007/s00024-020-02447-7.

Altiner Y, Söhne W, Güney C, Perlt J, Wang R, Muzli M (2013) A geodetic study of the 23 October 2011 Van, Turkey earthquake. Tectonophysics 588:118-134. doi.org/10.1016/j.tecto.2012.12.005.

An M, Feng M, Long C (2010) Deep ruptures around the hypocenter of the 12 May 2008 Wenchuan earthquake deduced from aftershock observations. Tectonophysics 491:96-104. doi:10.1016/j.tecto.2009.12.024

Baisch S, Ceranna L, Harjes H-P (2008) Earthquake cluster: what can we learn from waveform similarity? Bull. Seismol. Soc. Am. 98(6):2806–2814

Bayrak Y, Yadav RBS, Kalafat D, Tsapanos TM, Çınar H, Singh AP, Bayrak E, Yılmaz Ş, Öcal F, Koravos G (2013) Seismogenesis and earthquake triggering during the Van (Turkey) 2011 seismic sequence. Tectonophysics 601:163-176. doi:10.1016/j.tecto.2013.05.008

Benito B, Cepeda JM, Martinez Diaz JJ (2004) Analysis of the spatial and temporal distribution of the 2001 earthquakes in El Salvador. In: Rose WI, Bommer JJ, López DL, Carr MJ, Major JJ (eds) Natural hazards in El Salvador. The Geological Society of America Special Paper 375. Boulder, Colorado

Ben-Zion Y (2008) Collective behavior of earthquakes and faults: Continuum-discrete transitions, progressive evolutionary changes, and different dynamic regimes. Reviews of Geophysics. doi:10.1029/2008RG000260

Çınar, H. and Alkan, H., (2017) Crustal S-wave structure around the Lake Van region (eastern Turkey) from interstation Rayleigh wave phase velocity analyses, Turkish J. Earth Sci., 26: 73-90. doi:10.3906/yer-1605-13.

Çukur D, Krastel S, Demirel-Schluter F, Demirbağ E, Imren C, Nissen F, Toker M, PaleoVan-Working Group (2013) Sedimentary evolution of Lake Van (Eastern Turkey) reconstructed from high-resolution seismic investigations. International Journal of Earth Sciences (Geol Rundsch) 102:571-585. doi:10.1007/s00531-012-0816-x

Çukur, D., Krastel, S., Tomonaga, Y., Schmincke, H.-U., Sumita, M., Meydan, A.F., Çağatay, M.N., Toker, M., Kim, S.-P., Kong, G.-S. & Horozal, S., (2016) Structural characteristics of the Lake Van Basin, Eastern Turkey, from high-resolution seismic reflection profiles and multibeam echosounder data: Geologic and tectonic implications, *Int. J. Earth Sci. (Geol Rundsch),* 106**,** 239-253.

Dewey JF, Hempton MR, Kidd WSF, Şaroğlu F, Şengör AMC (1986) Shortening of continental lithosphere: The neotectonics of Eastern Anatolia-a young collision. In: Coward MP, Ries AC (eds) Collision tectonics. Geological Society Special Publications, vol. 19. London, pp. 3-36

Doğan B, Karakaş A (2013), Geometry of co-seismic surface ruptures and tectonic meaning of the 23 October 2011 Mw 7.1 Van earthquake (East Anatolian Region, Turkey). J. Struct. Geol. 46:99-114

Doğan U, Demir DÖ, Çakir Z, Ergintav S. Ozener H, Akoğlu AM, Nalbant SS, Reilinger R (2014) Postseismic deformation following the Mw 7.2, 23 October 2011 Van earthquake (Turkey): Evidence for aseismic fault reactivation. Geophys. Res. Lett. 41:2334-2341. doi:10.1002/2014GL059291

Elliott JR, Copley AC, Holley R, Scharer K, Parsons B (2013) The 2011 Mw 7.1 Van (eastern Turkey) earthquake. J. Geophys. Res. Solid Earth 118:1-19. doi:10.1002/jgrb.50117

Emre O, Duman TY, Ozalp S, Elmacı H (2011) 23 Ekim 2011 Van depremi saha gozlemleri ve kaynak faya ilişkin on değerlendirmeler. MTA Jeoloji Etutler Dairesi. Ankara

Fielding EJ, Lundgren PR, Taymaz T, Yolsal-Çevikbilen S, Owen SE (2013) Fault-Slip source models for the 2011 M 7.1 Van Earthquake in Turkey from SAR Interferometry, Pixel Offset Tracking, GPS, and Seismic Waveform Analysis. Seismological Research Letters 84(4):579-593. doi: 10.1785/0220120164

Gorbatov A, Kennett BLN (2003) Joint bulk-sound and shear tomography for western Pacific subduction zones. Earth Planet Sci Lett 210:527–543

Gori, P.D., Akinci, A., Lucente, F.P., Kılıç, T., (2014), Spatial and Temporal Variations of Aftershock Activity of the 23 October 2011 M_w 7.1 Van, Turkey, Earthquake. *Bulletin of the Seismological Society of America*; 104 (2): 913–930. doi: https://doi.org/10.1785/0120130118

Görür N, Cağatay MN, Zabcı C, Sakınç M, Akkök R, Hande Ş, Örcen S (2015) The Late Quaternary Tectono-stratigraphic Evolution of the Lake Van, Turkey. Bull. Min. Res. Exp. 151:1-46

Gutenberg B, Richter CF (1944) Frequency of earthquakes in California. Frequency of earthquakes in California. Bulletin Seismological Society of America;34 : 185-188.

Gülen L, Pınar A, Kalafat D, Özel N, Horasan G, Yılmazer M, Işıkara AM (2002) Surface fault breaks, aftershocks distribution, and rupture process of the 17 August-1999 Izmit, Turkey, earthquake. Bulletin of the Seismological Society of America 92:230–244.

Harris RA, Simpson RW, Reasenberg PA (1995) Influence of static stress changes on earthquake locations in southern California. Nature 375:221-224

Hill DP (1977) A model for earthquake swarms. J. Geophys. Res. 82:347-352

Hino R, Ito S, Shiobara H, Shimamura H, Sato T, Kanazawa T, Kasahara J, Hasegawa A (2000) Aftershock distribution of the 1994 Sanriku-oki earthquake (Mw 7.7) revealed by ocean bottom seismographic observation. J. Geophys. Res. 105:21697-21710

Irmak TS, Doğan B, Karakaş A (2012) Source mechanism of the 23 October 603 2011 Van (Turkey) earthquake (Mw = 7.1) and aftershocks with its tectonic implications. Earth Planets Space doi:10.5047/eps.2012.05.002

Kalafat D, Kekovalı K, Akkoyunlu F, Ögütçü Z (2013) Source mechanism and stress analysis of 23 October 2011 Van Earthquake (Mw=7.1) and aftershocks. J Seismol. 18:371-384. doi:10.1007/s10950-013-9413-0

Kalafat D, Gürbüz C, Üçer SB (1987) Batı Türkiye'de Kabuk ve Üst Manto Yapısının Araştırılması. Deprem Araştırma Bülteni Sayı 59: 43–64 (in Turkish)

Karakaş A, Coruk Ö, Doğan B (2013) Engineering geologic assessment of the slope movements and liquefaction failures of the 23 October 2011 Van earthquake (Mw = 7.2). Nat. Hazards Earth Syst. Sci. 13:1113-1126. doi:10.5194/nhess-13-1113-2013

Ketin I (1977) A short explanation about the results of observations made in the region between Lake Van and Iranian border. Bulletin of Geological Society of Turkey 20:79-85

Khilyuk LF, Chilinger GV, Robertson JO, Endres B (2000) Gas migration: Events preceding earthquakes. Gulf Publishing Company Press, USA

King G, Nablek J (1985) Role of fault bends in the initiation and termination of earthquake rupture. Science 228:984-987

King GCP, Stein RS, Lin J (1994) Static stress changes and the triggering of earthquakes. Bulletin of the Seismological Society of America 84:935-953

Koçyiğit A (2012) New field and seismic data about the intraplate strike-slip deformation in Van region, East Anatolian plateau, E. Turkey. Journal of Asian Earth Sciences 62:586-605. doi:10.1016/j.jseaes.2012.11.008

KOERI (2011-2014) Boğaziçi University, Kandilli Observatory and Earthquake Research Institute. http://www.koeri.boun.edu.tr/

Kutoğlu HS, Toker M, Mekik C (2016) The 3-D Strain patterns in Turkey using Geodetic velocity fields from the RTK-CORS (TR) Network. Journal of African Earth Sciences 115:246-270. doi:10.1016/j.jafrearsci.2015.12.002

Lee WHK, Lahr JC (1972) HYPO71: a computer program for determining hypocenter, magnitude and first-motion pattern of local earthquakes, U.S. Geological survey open-file report, pp. 100

Lee WHK, Valdes CM (1985) HYPO71PC: A Personal Computer Version of the HYP071 Earthquake Location Program, USGS, Open File Report, pp. 1–28

Mackenzie, D., Elliott, J.R., Altunel, E., Walker, R.T., Kurban, Y.C., Schwenninger, J.-L., and Parsons, B., (2016), Seismotectonics and rupture process of the Mw 7.1, 2011 Van reverse-faulting earthquake, eastern Turkey, and implications for hazard in regions of distributed shortening , *Geophysical Journal International*, 10.1093/gji/ggw158, **206**, 1, 501-524.

Moro M, Cannelli V, Chini M, Bignami C, Melini D, Stramondo S, Saroli M, Picchiani M, Kyriakopoulos C, Brunori CA (2014) The October 23, 2011, Van (Turkey) earthquake and its relationship with neighbouring structures. Sci. Rep. doi:10.1038/srep03959

Ohnaka M, Kato A (2007) Depth dependence of constitutive law parameters for shear failure of rock at local strong areas on faults in the seismogenic crust. J. Geophys. Res. doi: 10.1029/2006JB004260

Omori F (1884) On the aftershocks of earthquakes. Journal College of Sciences, Imperial University 7:111-200

Özalp, S., Aydemir, B.S., Olgun, Ş., Şimşek, B., Elmacı, H., Evren, M., Emre, Ö., Aydın, M.B., Kurtuluş, O., Öcal, F., Can, A.Z., Yanmaz, M.N., Apa, R. & Duman, T.Y., (2016) Tectonic deformations in the quaternary deposits of the Lake Van (Edremit Bay), Eastern Anatolia, Turkey, *Bull. Min. Res. Exp.,* 153.

Reasenberg P, Simpson R (1992) Response of regional seismicity to the static stress change produced by Loma Prieta Earthquake. Science 255:1687-1690

Salah, M.K., Şahin, Ş., Aydin, U., 2011. Seismic velocity and Poisson's ratio tomography of the crust beneath East Anatolia. Journal of Asian Earth Sciences 40 (2011) 746–761. doi:10.1016/j.jseaes.2010.10.021.

Salah, M.K., Şahin, Ş., Destici, C., 2007. Seismic velocity and Poisson's ratio tomography of the crust beneath southwest Anatolia: an insight into the occurrence of large earthquakes. Journal of Seismology 11, 415–432. doi:10.1007/s10950-007-9062-2.

Scholz CH (2002) The mechanics of earthquakes and faulting, 2nd edn. Cambridge University Press, Cambridge

Şengör AMC, Görür N, Şaroğlu F (1985) Strike-slip faulting and related basin formation in zones of tectonic escape. Turkey as a case study in Strike-slip faulting and basin formation. In: Biddle KT, Christie-Blick N (eds) Strike-slip deformation, basin formation and sedimentation. Special Publication of Society of Economic Paleontologists and Mineralogists, vol. 37. Tulsa, Oklahoma, pp 227-264

Şengör AMC, Özeren MS, Genç C, Zor E (2003) East Anatolian high plateau as a mantle-supported, north-south shortened domal structure. Geophysical Research Letters 30(24):8045. doi:10.1029/2003GL017858

Şengör AMC, Özeren MS, Keskin M, Sakınç M, Özbakır AD, Kayan İ (2008) Eastern Turkish high plateau as a small Turkic-type orogen: Implications for post-collisional crust-forming processes in Turkic-type orogens. Earth-Science Reviews 90(1-2):1-48

Stein RS (1999) The role of stress transfer in earthquake recurrence. Nature 402:605-609

Stein RS, Lisowski M (1983) The Homestead Valley earthquake sequence, California: Control of aftershocks and postseismic deformations. Journal Geophysical Research 88: 6477-6490

Strehlau J (1986) A discussion of the depth extent of rupture in large continental earthquakes. In: Das S, Boatwright J, Scholz CH (eds) Earthquake source mechanics. American Geophysical Union. Washington, pp 131-145

Toker M (2011) Tectonic and magmatic structure of Lake Van basin and its structural evolution, Eastern Anatolia Accretionary Complex (EAAC), E-Turkey. PhD thesis, Istanbul Technical University

Toker, M., Şahin, Ş. (2019). Crustal Poisson's ratio tomography and velocity modeling across tectono-magmatic lake regions of Eastern Anatolia (Turkey): New geophysical constraints for crustal tectonics, Journal of Geodynamics, 131, 101651, 1-28.

Toker M, Şengör AMC (2011) Van Gölü havzasının temel yapısal unsurları, tektonik ve sedimanter evrimi. Doğu Türkiye İTÜ Dergisi/D, Mühendislik 10(4):119-130.

Toker M, Ecevitoğlu GB (2012a) Van Gölü havzasının tektonik ve sismolojik özellikleri (6000 artçı deprem ve 180 günlük sismolojik ve sismotektonik modellenmesi), 1st edn. Anadolu University Publications, ISBN 978-975-06-1109-4, Eskişehir, Turkey (in Turkish).

Toker M, Ecevitoğlu GB (2012b) Shallow seismicity of the Van earthquake (M_L, 7.2, 23 October 2011, Eastern Anatolia): monitoring and analysis of the seismic data. In: Proceedings of the national conference with international participation "Geosciences 2012", Bulgarian Geological Society (BGS), Sofia, 13-14 December 2012

Toker M (2013) Time-dependent analysis of aftershock events and structural impacts on intraplate crustal seismicity of the Van earthquake (Mw 7.1, 23 October 2011), E-Anatolia. Central European Journal of Geosciences. 5:423-434. doi: 10.2478/s13533-012-0141-8

Toker M (2014) Discrete characteristics of the aftershock sequence of the 2011 Van earthquake. Journal of Asian Earth Sciences 92:168-186. doi:10.1016/j.jseaes.2014.06.015.

Toker M (2015) Multi-clusteral nature of the 2011 Van earthquake aftershock sequence in the accretionary region of Eastern Anatolia. In: Efe R, Bizzarri C, Cürebal İ, Nyusupova GN (eds) Environment and ecology at the beginning of 21st century. St. Kliment Ohridski University Press, Sofia

Toker, M., (2017) The b-value analysis of aftershocks 170 days after the 23 October 2011 Van earthquake (Mw, 7.1) of the Lake Van basin, Eastern Anatolia: A new perspective on the seismic radiation and deformation characteristics. *in Earthquakes - Tectonics, Hazard and Risk Mitigation*, ed. Zouaghi, T.

Toker, M., Sengör, A.M.C., Demirel-Schluter, F., Demirbağ, E., Çukur, D., Imren, C., Niessen, F. & Group, P.-W., (2017) The structural elements and tectonics of the Lake Van basin (Eastern Anatolia) from multi-channel seismic reflection profiles, *J. Afr. Earth Sci.,* 129**,** 165-178.

Turkoglu, E., Unsworth, M. J., Caglar, I., Tuncer, V. and Avsar, U. (2008) Lithospheric structure of the Arabia-Eurasia collision zone in eastern Anatolia: Magnetotelluric evidence for widespread weakening by fluids? Geology, 36, 619–622.

Turkoğlu, E., Unsworth, M., Bulut, F., Çağlar, İ. (2015) Crustal structure of the North Anatolian and East Anatolian Fault Systems from magnetotelluric data, Physics of the Earth and Planetary Interiors, doi: http://dx.doi.org/10.1016/j.pepi.2015.01.003.

Utkucu M (2006) Implications for the water-level-change triggered moderate (M≥4.0) earthquakes in Lake Van basin, Eastern Turkey. Journal of Seismology 10:105–117. doi: 10.1007/s10950-005-9002-y

Utkucu M (2013) 23 October 2011 Van, Eastern Anatolia, earthquake (Mw 7.1) and seismotectonics of Lake Van Area. Journal of Seismology 7(5):23-33

Utkucu M, Durmuş H, Yalçın H, Budakoğlu E, Işık E (2013) Coulomb static stress changes before and after the 23 October 2011 Van, eastern Turkey, earthquake (Mw = 7.1): Implications for the earthquake hazard mitigation. Natural Hazards and Earth System Science 13:1-14. doi: 10.5194/nhess-13-1-2013

Wessel P, Smith WHF (1998) New, improved version of the Generic Mapping Tools released. EOS 79:579

Yaginuma T, Okada T, Umino N, Hasegawa A (2005) Asperity of the 2005 off Miyagi earthquake (M7.2) estimated by waveform inversion [in Japanese]. Program Abstr. Seism. Soc. Japan, PM16

Yılmazer M (2003) Deprem kaynak parametrelerinin On-line Belirlenmesi. İstanbul Üniversitesi, Fen Bilimleri Enstitüsü, Yüksek Lisans Tezi, 47 s, İstanbul (Turkish)

Zor, E. (2008) Tomographic evidence of slab detachment beneath eastern Turkey and Caucasus. Geophysical Journal International, 175, 1273–1282.

Zor, E., Sandvol, E., Gurbuz, C., Turkelli, N., Seber, D. and Barazangi, M. (2003) The crustal structure of the East Anatolian plateau (Turkey) from receiver functions. Geophysical Research Letters, 30, 8044, doi: 10.1029/2003GL018192.